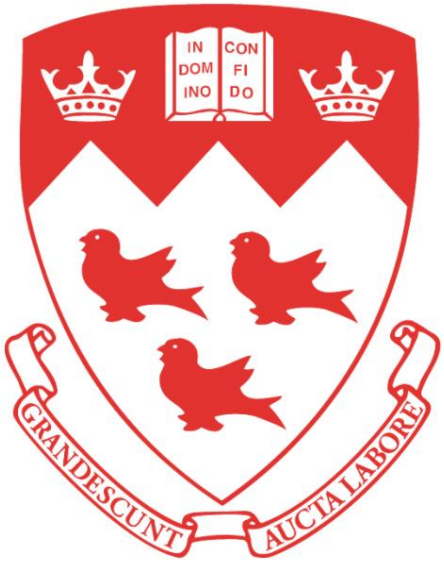

Finite Element and Analytical Models to Predict the Strength of Carbon-Epoxy Laminates with Defects

Pranshul Thakur

Supervisor: Prof. Larry Lessard

A thesis submitted to McGill University in partial fulfilment of the requirements of the Undergraduate Honours Program.

Department of Mechanical Engineering

McGill University

December 7th, 2020

A happy and memorable moment of meeting with Prof. Lessard virtually and a sign of the times that we live in.

Abstract

Automated fibre placement (AFP) manufacturing technique is widely used in aerospace industries to create large and complex composite parts. In this method, the layup is done by a computer-controlled robotic arm, which places tows of uncured pre-impregnated carbon fibres over a specified path. AFP is a fast and efficient process as it paves the way to automation in the composites industry. However, this process results in defects in the manufactured parts which are not seen in other manufacturing techniques. The most common of AFP induced defect is the half gap/half overlap defect, caused due to a misaligned tow. Industries rely primarily on experiments to determine the impact of these defects on mechanical strength of the structures. However, experimental investigations are costly and require significant time.

The research presented in this thesis aims to develop finite element and analytical models which can predict the strength of composite structures containing half gap/half overlap defects. Microscopy analysis is performed on structures with defects to gain an understanding about the internal structure of defects and is included in the simulations to closely model defects in real world. The effect of different parameters of defects on the strength are also investigated, such as defect size, number and orientation. The model is verified with experiments and it is in good agreement with the results for tensile strengths. However, it needs to be improved further to accurately predict compressive strengths.

Résumé

La technique de fabrication du placement automatisé des fibres (abrégé AFP pour *Automated Fibre Placement*) est largement utilisée dans les industries aérospatiales pour créer des pièces composites grandes et complexes. Dans cette méthode, la superposition est effectuée par un bras robotisé commandé par ordinateur, qui place des câbles de fibres de carbone pré-imprégnés non durcis sur un chemin spécifié. AFP est un processus rapide et efficace car il ouvre la voie à l'automatisation dans l'industrie des composites. Cependant, ce procédé entraîne des défauts dans les pièces fabriquées qui ne sont pas visibles dans d'autres techniques de fabrication. Le défaut le plus courant induit par l'AFP est le défaut demi-écart / demi-chevauchement, causé en raison d'un câble mal aligné. Les industries s'appuient principalement sur des expériences pour déterminer l'impact de ces défauts sur la résistance mécanique des structures. Cependant, les investigations expérimentales sont coûteuses et nécessitent un temps considérable.

La recherche présentée dans cette thèse vise à développer des modèles de simulation capables de prédire la résistance de structures composites contenant des défauts demi-écart / demi-chevauchement. L'analyse microscopique est effectuée sur des structures présentant des défauts pour acquérir une compréhension de la structure interne des défauts et est incluse dans les simulations pour modéliser étroitement les défauts dans le monde réel. L'effet de différents paramètres de défauts sur la résistance est également étudié, tels que la taille, le nombre et l'orientation des défauts. Le modèle est vérifié expérimentalement et est en bon accord avec les résultats pour les résistances à la traction. Cependant, il doit encore être amélioré pour prédire avec précision les résistances à la compression.

Acknowledgements

I would like to thank Professor Larry Lessard for his guidance and invaluable mentorship. He has immensely improved my knowledge in composites and has helped me throughout the research. I am extremely grateful to him for providing me an opportunity to work on the interesting project of AFP. I would also like to thank the members from the Structures and Composite materials laboratory. The weekly group meetings were immensely helpful in getting acquainted with the field. I would also like to thank previous masters students, Vincent Cadran and Daniel Del Rossi for the experimental data.

This research project was done in collaboration with our funding partners, Bell Textron Canada Limited and National Research Council, Aerospace Manufacturing Technology Centre (NRC-AMTC). Funding from the Natural Science and Engineering Research Council of Canada (NSERC) is gratefully acknowledged, as well as cooperation from Center for Research on Polymers and Composites (CREPEC).

Table of Contents

List of Figures

List of Tables

List of Equations

1. Introduction

1.1 Composite materials and AFP

Composite materials are made by a combination of two or more materials to form heterogeneous structures with desired material properties. Usually, they consist of fibres casted in a resin. Such materials have different strengths and modulus in different directions. Laminated composites are an important class of advanced composite materials which are formed by stacking layers of different fiber orientations to form a laminate with required properties. The material is then cured in an autoclave, which subjects the uncured laminate to high pressure and temperature.

Carbon-epoxy laminates (composed of carbon fibres in epoxy matrix) are an important class of high performance composite materials that are widely used in aerospace industries. They offer high strength-to-weight ratio and are resistant to corrosion. Several manufacturing techniques are used to create such materials. A conventional approach is hand layup, in which plies of composite materials are manually laid down on a mould before curing. This process is slow and is subject to errors made by humans. With the onset of automation, many composite industries are using Automated Fibre Placement (AFP) process to manufacture composite parts. In this method, a computer-controlled robot arm lays down tapes of composite materials on the mould in a specified direction, as shown in Figure 1.1.

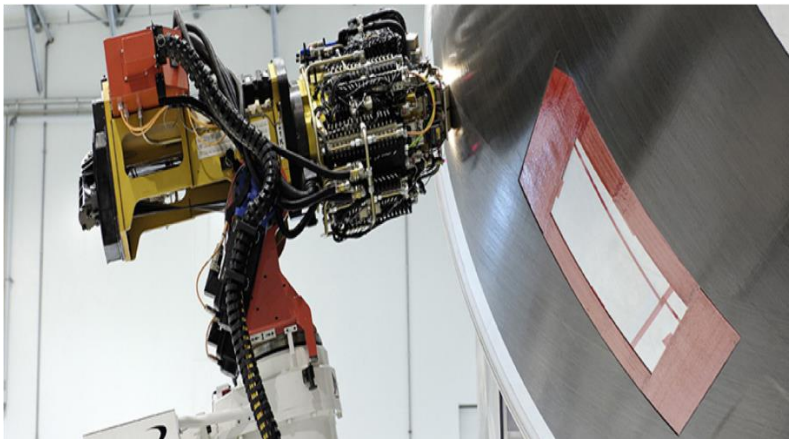

Figure 1.1: AFP machine [1]

A roller and a hot torch/laser are attached to the robot head to apply pressure and heat on the tape as it is laid down, as shown in the schematic in Figure 1.2.

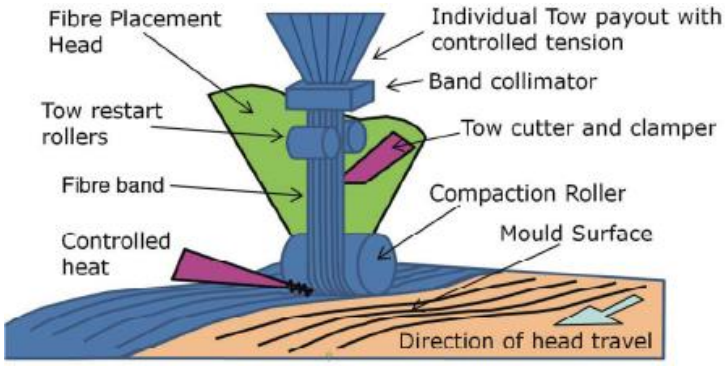

Figure 1.2: Schematic of the AFP machine's head [2]

After the tows are laid side by side to form the stack, the entire laminate is cured. AFP is a fast and efficient process for manufacturing complex large parts. However, this method causes defects not seen in other manufacturing techniques. The tows can get twisted during layup or can have resin rich regions creating bulks. The most common defect associated with the AFP is a half gap/half overlap due to the misalignment of a tow [3]. The gap region of the misaligned tow is filled by

resin and the overlap region is rich in fibres. This defect type can have detrimental effects on the structural strength of AFP manufactured composites.

1.2 Motivation and Objectives

Parts created by AFP contain half gap/half overlap defects caused by a misaligned tow. To reduce the amount of defects, plies are checked after the layup of each layer and defects are fixed manually. This reduces the advantage offered by the AFP in terms of speed and automation. Due to their directional properties, strengths of composites with defects is difficult to analyse theoretically. Hence, industries rely on experiments to determine the strengths of laminates with defects and the acceptable level of defects in a part. Such experiments are costly and time consuming. An efficient simulation model to predict the strengths of composite structures with defects can significantly reduce the costs to perform experiments. Several researchers have been working on developing different simulation models. However, as shown by a detailed literature review in the introduction of Chapter 2, the models do not model defects as seen in the industries. Most defects encountered are half gap half overlap which are finite in size.

The goal of this research is to develop models to predict the strength of laminates containing half gap/ half overlap defects which match the defects as seen in industries. The internal structure of defects and the effect of different defect parameters (i.e. number, size and orientation of defects) are also investigated using the models.

1.3 Outline of research

As noted in the introduction, half gap/half overlap defects are the most common defect types observed in AFP manufactured parts. To gain an understanding about the effect of these defects, the internal structure of defects has to be understood. In Chapter 2, detailed microscopy analysis is performed on several carbon-epoxy samples with defects. Various regions of defects and their properties are identified. Tensile and compressive tests (performed by previous graduate students, [1,4]) are also presented for completeness.

In Chapter 3, various models to predict strengths are investigated. Models based on cohesive interaction and cohesive elements (made by previous graduate students, [1,4]) are compared. Finally, a model is presented to generate waviness in plies as seen in the microscopy.

In Chapter 4, an analytical model is presented which uses waviness from the FEA simulation of Chapter 3 and predicts the strengths of laminates with defects. The model is in good agreement with experiments for the tensile tests. Using this model, defect parameters (i.e. number, size and orientation of defects) are varied and the corresponding tensile strengths are obtained. Finally, with these additional data points, the effect of different parameters and the most important defect parameter are identified.

1.4 Important note

Chapters 2 and 3 are written in manuscript format. Chapter 2 and 3 form a two-part manuscript for a journal. At the time of writing this thesis, the papers were not yet submitted. They will soon be submitted to the journal "Composite Structures". The collaborators on the papers are indicated on the manuscripts at the beginning of Chapters 2 and 3.

References

1. Cadran, V., *Effect of Defects made by Automated Fibre Placement Process on Carbon/Epoxy Composite Structures.* in *Mechanical Engineering*. 2019, McGill University: Montreal.
2. Li, X., S.R. Hallett, and M.R. Wisnom. *Modelling the effect of gaps and overlaps in automated fibre placement (AFP)-manufactured laminates*. Science and Engineering of Composite Materials, 2015. 22(2): p. 115-129.
3. SA2GE Project. in *Composite Fuselage Structures*. 2015, Bell Helicopter Textron Canada Limited.
4. Rossi, D.D., *Effect of Half Gap/Overlap Defects on the Strength of Composite Structures Fabricated with Automated Fiber Placement Methods*, in *Mechanical Engineering*. 2018, McGill University: Montreal.

2. Experimental investigation of the effect of half gap/half overlap defects on the strength of composite structures fabricated using automated fibre placement (AFP) method.

Del Rossi, D.[1], Cadran, V.[1], Thakur, P.[1], Palardy-Sim, M.[2], Lapalme, M.[3] and Lessard, L.[1]

[1] Department of Mechanical Engineering, McGill University, Montreal, Quebec Canada H3A 0C3

[2] National Research Council Canada, Aerospace Manufacturing Technology Centre, 2107 ch. de la Polytechnique Montreal, Quebec, Canada, H3T 1J4

[3] Bell Textron Canada Limited, 12800 rue de l'avenir, Mirabel, Québec, Canada J7J 1R4

Abstract

The Automated Fibre Placement (AFP) process has gained traction as an efficient manufacturing method for large and complex composite structures. An AFP machine uses a computer-controlled arm with a head at the end capable of constant placement of uncured pre-impregnated carbon fibre tows grouped together to form bands. While AFP offers benefits through automation, certain defects inherent to the manufacturing method are induced. Primary defects observed by the aerospace industry are misaligned tows, often the result of trying to steer the tows. This defect occurs when a tow deviates from the intended path causing a combination of both side-to-side gaps and overlaps. In this first of a two-part paper, we experimentally investigate the effects of steered tow defects on the mechanical performance of carbon-epoxy composite structures made with AFP. The orientation, size and number of steered tow defects embedded in the laminates are varied, and their mechanical effects are examined by static tension, static compression and fatigue tests.

Simulation models to predict the performance of composite structures with defects are investigated in the second paper of this two-part paper. The major experimental result is that compression is more critical than tension with the largest strength reductions reaching 25% and 10%, respectively. The configuration of the defects has a significant effect on the results. For example, the greater the number of defects, the lower the compressive strength for 45° oriented defects but the opposite is observed for 90° oriented defects. An increased defect width leads to a higher compressive strength in 45° configurations while it is the opposite for tensile tests. The experiments give insight into the behaviour of AFP panels and help to understand their failure modes.

2.1 Introduction

Composite structures are used extensively in the aerospace industry due to their high strength- to-weight ratio. Automated Tape Laying (ATL) and Automated Fibre Placement (AFP) are the two main automated technologies that use advanced composite laminates from unidirectional (referred as UD) pre-impregnated fibres (prepregs) [1,2]. However, the AFP machines are not perfect. They may create defects in some areas, which end up being embedded in the laminate [3]. Corresponding methods to detect and repair the defects are inefficient and time consuming [4]. Tow mislocation defects are particularly interesting because they cause adjacent gap/overlaps, important in the understanding of the performance of AFP manufactured parts. Among the various types of defects caused by AFP process, adjacent gap/overlap defects are the most common, as shown by Bell Textron Canada Limited in a study in 2015 [5]. Adjacent gap/overlap defects represent more than 57% of all defects that have been counted on a representative helicopter part (other types of defects encountered include wrinkling, bridging and other design related defects). It occurs when a tow is misaligned, as shown in Figure 2.1.

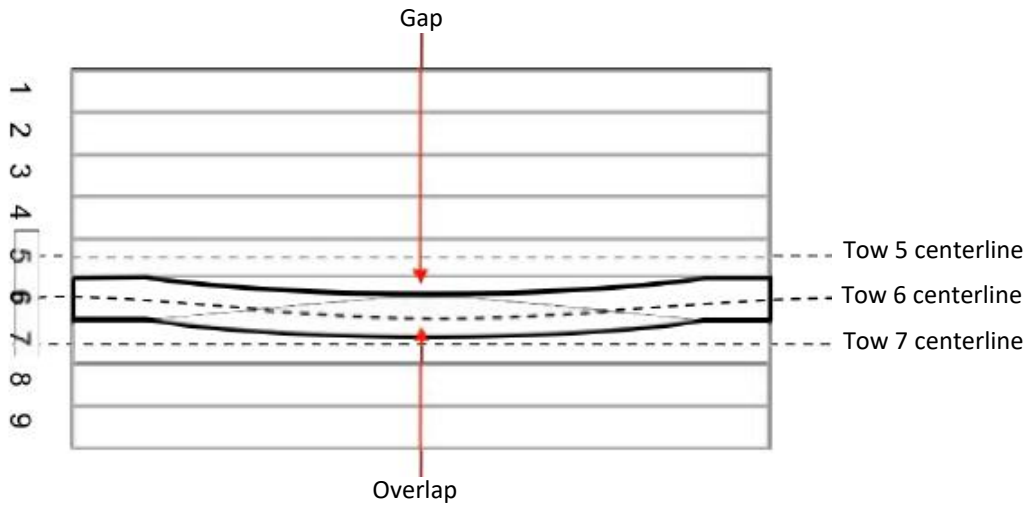

Figure 2.1: Tow misalignment creating gap/overlap defect

These defects can affect mechanical performance of the structures. Recent research developments were made on the effect of gap and overlap defects. For instance, Sawicki and Minguet [6] studied the reduction in strength in compression of composite carbon fibres specimens with embedded gaps aligned at a 90° ply orientation. Size and location of defects were reported and it appears that coupons with defects of at least 0.03 in (0.762 mm) width had a strength reduction of up to 27%. Wider defects did not have larger strength reductions. Notched and unnotched specimens achieved similar performance. They failed because of significant out-of-plane waviness according to the authors' observations because waviness leads to buckling instability. In 2010 an experimental study was carried out by Croft where a variety of AFP related defects was tested [7]. In the study, defects were placed at the center of the laminate and went through the entirety of the part. The material used for the laminate was CYCOM 5276-1 with a layup of $[45/0/-45/90]_{2S}$ and the coupons where made with soft tooling (no upper caul plate). The tests show that there is less than a 5% difference when any type of defect is introduced into the laminate. However, the half gap/overlap configuration had the worst effect. It is important to note however that having two defects directly on top of each other as it is the case here is not common, especially if it goes from one end of the coupon to the other. Regardless, these results show that in general more gaps (such as the type of gap/overlap shown in Figure 2.1) would be needed in order to have a larger effect on the strength. Elsherbini and Hoa [8, 9] studied the effect of gaps on fatigue behaviour of unidirectional carbon/epoxy laminates. They concluded that the effect of gaps depends on the maximum applied stress during fatigue: as the maximum applied stress in the fatigue cycle increases, the effect of gaps becomes more severe. Turoski [10] investigated the effects of isolated and staggered gaps on the tensile and compressive strengths of notched and unnotched quasi-isotropic laminates. The author concluded that since half gap / half overlap defects show strong

waviness, the prediction of mechanical performance is more difficult to assess A study by Nguyen MH et. al. [11] has shown that the width of the gap decreases and the width of the overlap increases during compaction of the laminate containing gap and overlap defects. M. Ghayour et al. [12] investigated the effect of fibre tow gaps (created using AFP) on the impact response of carbon/epoxy laminates. While performing microscopy analysis on the laminates, they concluded that the fibre tow gaps were filled due to fibre and resin movement during the curing process. Fayazbakhsh et al. [13,14,15] studied the effects of single gaps and single overlaps with finite element modelling using a new method called the "defect layer method". Defects were defined with different material properties and ply thickness variation. For instance, a gap was defined as a rich resin region with resin properties. For overlaps, the layer had the same properties everywhere but the local thickness was increased. Through optimization algorithms buckling and in-plane stiffness were studied. Gaps reduced buckling capability by an average of 12% and overlaps increased it by an average of 30%. Gaps reduced in-plane stiffness by an average of 14% while overlaps increase it by an average of 10%. This work [13,14,15] has been verified by experiments.

The literature on fatigue for composite materials is extensive. However, the effects of AFP manufacturing defects on the fatigue response of composite laminates have barely been studied [9]. Evidence of damage can be detected in one of the many forms of failure: matrix cracking, fibre-matrix cracking, delamination, void growth and fibre cracking. For cross-ply laminates, damage is initiated with delamination at the edges and then it propagates. Matrix cracks appear before fibre breakage at failure [16,17]. Fatigue life decreases when the amplitude increases at constant mean stress. Fatigue life also decreases when either temperature or frequency increases [18,19,20]. Colombo and Vergani [21] studied the effect of delamination on glass fibre composites

and found that the strength of such laminates with embedded delamination does not change but the fatigue life does change. The fatigue life was shortened much more at high levels of applied fatigue stress; thus, the defect is activated in fatigue at high stress levels. Recently, Margoni et al. [22] studied the compressive fatigue behavior of woven carbon epoxy laminates. They concluded that bundle waviness had a large influence on the damage mechanisms and the fatigue life of laminates for tension-compression and compression-compression loadings. They showed that the loss in stiffness was small until the final failure in all cases. M. Thor et al. [23] studied the causes of wrinkle formation in fibre-reinforced composites i.e. the geometry and manufacturing processes, and gave recommendations to minimize the out of plane waviness.

Though intensive research has been done on the effect of gaps and overlaps, the impact of the adjacent gap/overlap defect on the mechanical performance of the laminates has not been extensively studied. Most of the research has been done on the defects that go through the entire coupon. These defects do not follow the actual geometry of a misaligned tow which are the most commonly encountered defects in industries according to [5]. In this paper, we present our experimental investigation to determine the affect of half gap/ half overlap defect configuration created by a misaligned tow on mechanical performance of the laminates. Effect of defect size, orientation and number of defects are investigated. The goal is to help aerospace companies better understand the effect of half gap/half overlap defects on the mechanical performance and hence plan their layups and production accordingly.

2.2 Parameters and configurations of coupons used

2.2.1 Coupon dimensions, layup and defect geometry

The coupons used in this study are carbon fibre-reinforced epoxy composite laminates following a Quasi-Isotropic layup of 16 plies to which one ply of fabric composite is added at the top and bottom, leading to an 18 ply-laminate. Fabric woven plies are added because it is a standard practice developed in industry by the industrial partner of this work. The unidirectional prepreg is T800S/3900-2 and the cross ply woven fabric is T400/3900-2. The layup is $[45F/(-45T/0T/45T/90T)_2]_s$ where "F" stands for Fabric and "T" stands for Tape.

Coupons are manufactured using Automated Fibre Placement (AFP) layup and autoclave curing at the Canadian National Research Council's Aerospace Manufacturing Technology Centre in Montreal, Canada. The defect geometry chosen for the current set of experiments is commonly seen in industry as the closest representation possible of a true half gap / half overlap defect made by an AFP machine [5]. This misaligned tow momentarily crosses over onto the adjacent tow within the same ply. This adds both local in-plane and out-of-plane waviness in the specimen. The half gap / half overlap defect ends up having a trapezoidal shape as shown in Figure 2.2. The lengths of the defects were fixed so that they would fit in the largest available test fixture. The total length of the defects was 2.5 in (63.5 mm) and the width was varied between 0.05 in and 0.1 in (1.27 mm and 2.54 mm).

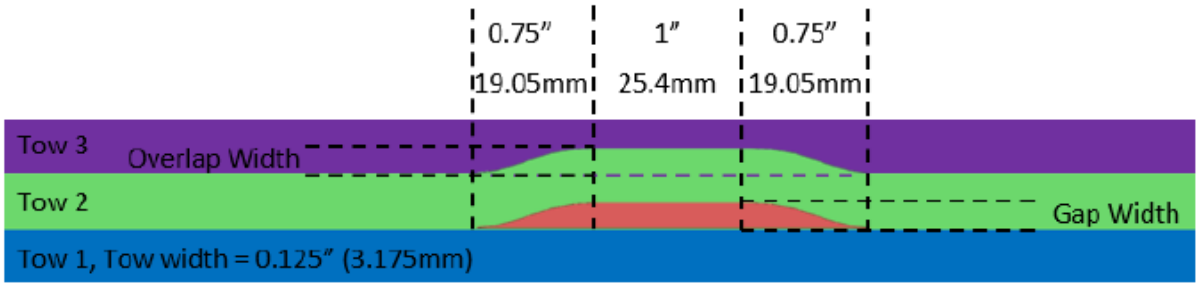

Figure 2.2: Top view of half gap/half overlap defect dimensions

There are infinite configurations of defects that can be introduced into a laminate. The goal of this paper is to capture the effects of the gap/overlap defects with some common configurations that may be seen in industry (combinations of gap/overlap defects). This geometry represents the pre-cured defect geometry before compaction and heat are applied on the panels. Thus, the dimensions shown in Figure 2.2 will be different post-cure as it has been observed to change in the microscopy images due to shear flow.

Dimensions of coupons have been chosen by consideration of ASTM D3039 [24] for static tension and ASTM D6484 [25] for static compression and cyclic fatigue. Two sizes of coupons are defined (see Figure 2.3 and Figure 2.4). On these two figures, the grip section corresponds to static tension ASTM D3039 [24] loading type while ASTM D6484 [25] has an anti-buckling fixture with a window at the location of defects only as shown in Figure 2.5. Two ASTM D6484 fixtures of dimensions corresponding to those of coupons shown in Figure 2.3 and Figure 2.4 were used for static compression and cyclic fatigue loading.

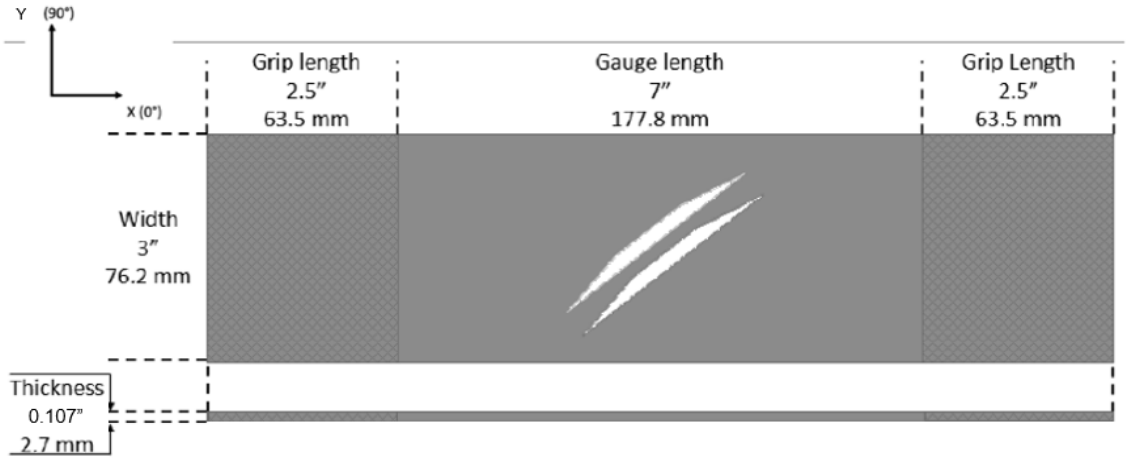

Figure 2.3: Dimensions for 90° coupons, 45° coupons and mixed orientations coupons

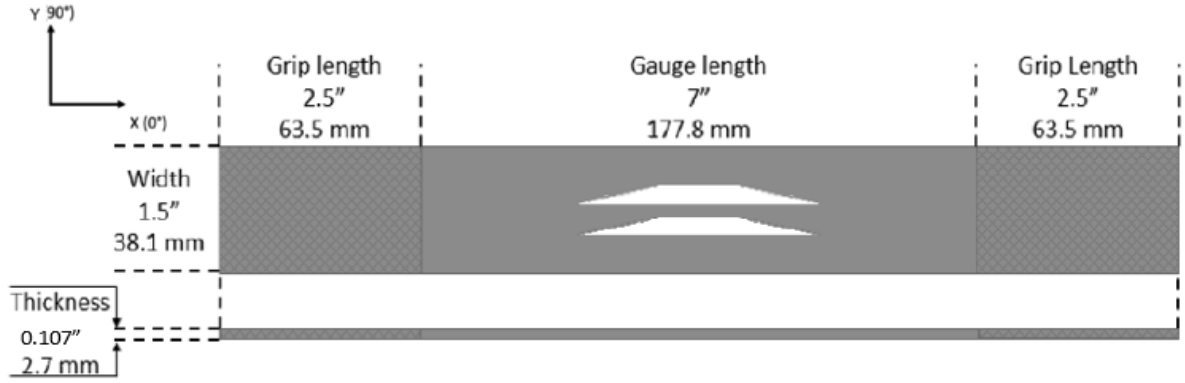

Figure 2.4: Dimensions for 0° coupons and defect-free coupons

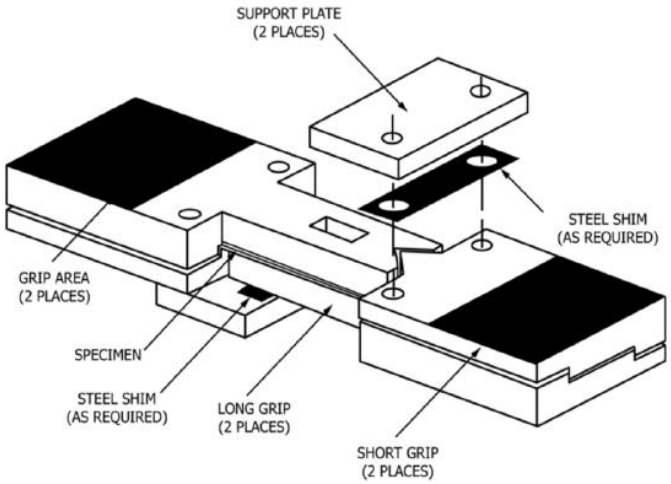

Figure 2.5: Anti-buckling fixture ASTM D6484 [25] for static compression and fatigue

Coupons with configurations that have 0° oriented defects and defect-free coupons have a smaller width than coupons with 90° and 45° oriented defects to reduce the required material quantity for manufacturing. Widths of the coupons were chosen in accordance with a study by Lessard et. al [26] where it was shown that a laminate no longer sees the edge effect singularity at a distance from the edge of 0.9 times the thickness. To safely neglect edge effects, the coupons were dimensioned such that the embedded defects were always further from the coupon's edges by more 1.5 times the thickness.

2.2.2 Coupon configurations used for tension, compression and fatigue tests

Coupons with varying defect configurations were used for tests. Three different test categories were defined: compression, tension and fatigue loading conditions. In tension and compression, 5 coupons of each configuration were manufactured while 9 coupons per configuration were made for fatigue tests. These numbers of coupons per configuration correspond to a minimal statistic population needed to study the variation of the results. Also, for fatigue, coupons were tested at different stress levels to build S-N curves of each configuration. Each test plan was composed of configurations that vary the following parameters:

a) total number of defects
b) width of defects
c) orientation of defects

The coupon configurations used for static compression and tension are shown in Figure 2.6 while the configurations for the fatigue tests are shown in Figure 2.7.

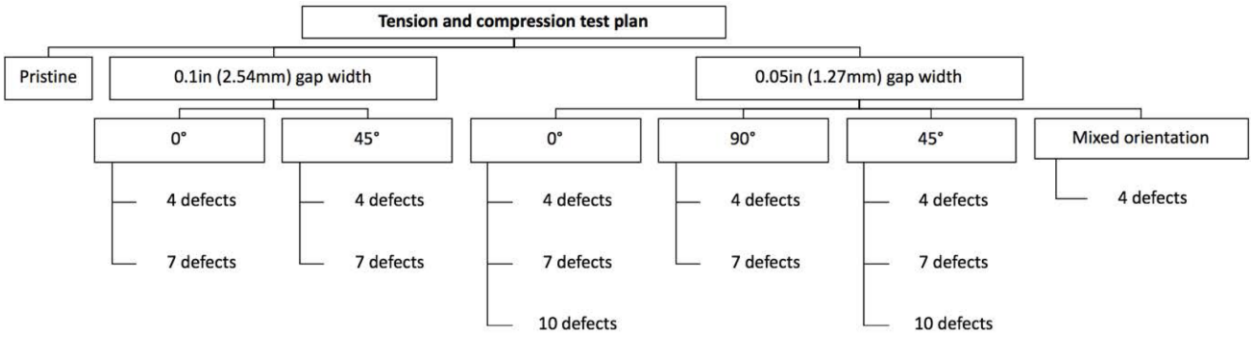

Figure 2.6: Defect configurations for static compression and tension

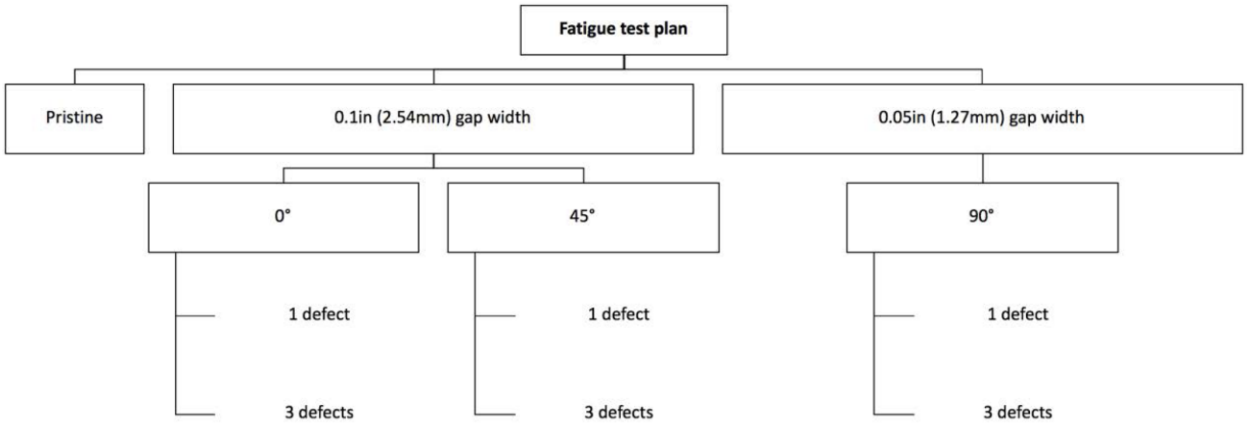

Figure 2.7: Defect configurations for cyclic fatigue

Hap / half overlap defects are embedded at the middle of the coupons along their length. Locations of defects through the thickness are shown in Figure 2.8 and Figure 2.9. The defects follow a stagger pattern through the thickness which helps keeps a certain balance in the defected coupons to limit unwanted out-of-plane effects.

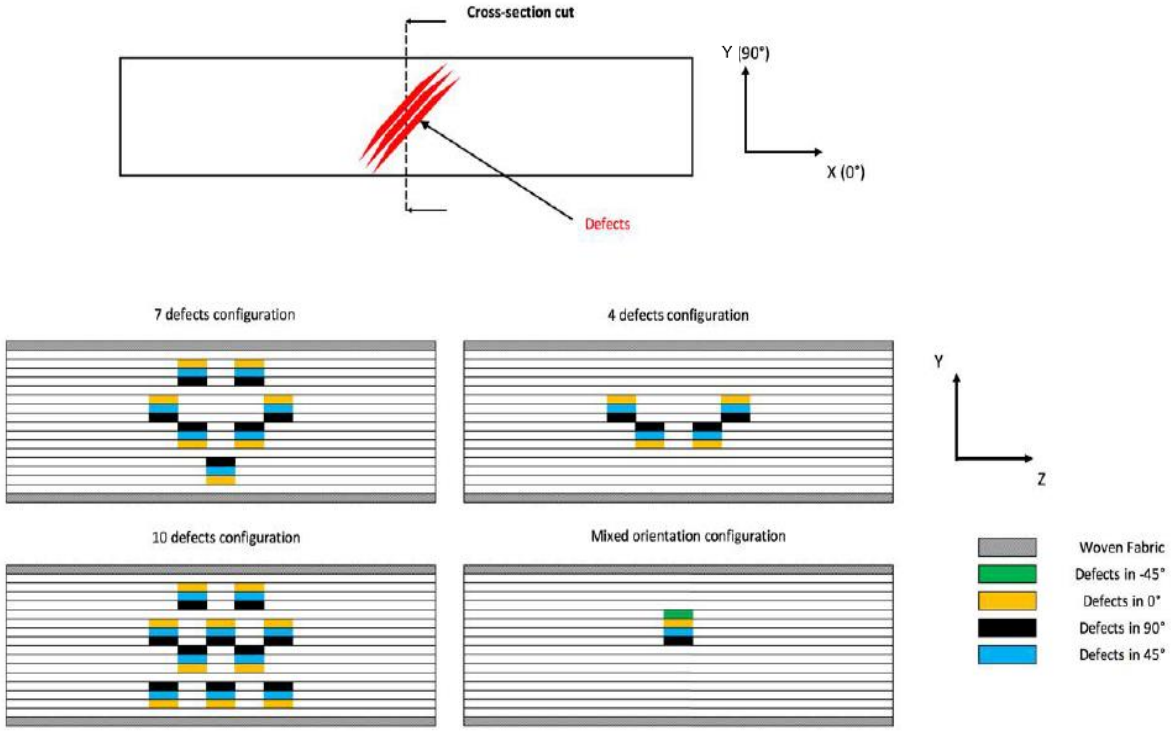

Figure 2.8: Locations of defects for static tension and compression tests. Note that for 4, 7 and 10 defect configurations, only one defect angle is used per specimen (3 defects shown to save space)

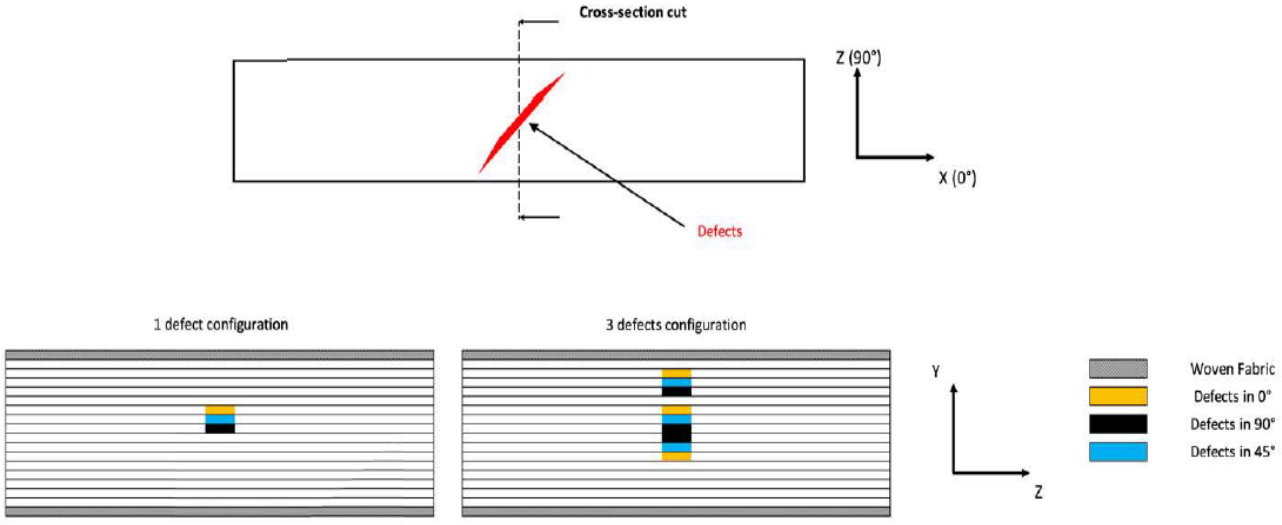

Figure 2.9: Locations of defects for cyclic fatigue tests. Note that for 1 and 3 defect configurations, only one defect angle is used per specimen (3 defects shown to save space)

2.3 Manufacturing and quality control

2.3.1 Layup, defect insertion and cure cycle

A 6-axis gantry type AFP machine was used to lay down composite prepreg on a flat polished stainless-steel metal table. Half gap / half overlap defects (as depicted in Figure 2.1) are manually embedded in the panels at specific locations. Layup and cure were performed using the manufacturer's suggested cure cycle. Manufacturing parameters are summarized in Table 2.1. A total of 194 coupons were cut from panels for tension, compression and fatigue testing.

Table 2.1: Manufacturing parameters of the AFP machine

Speed (mm/s)	Pressure (kg)	Nozzle (°C)	Creel (°C)	Room (°C)	Humidity (%)
140	25	100	14	23	34 – 42

Cure cycle

The cure cycle shown in Figure 2.10 was provided by the resin manufacturer. The finished panels were moved from the table where they were manufactured and placed between polished caul plates. The bagging process is shown in Figure 2.11. Bag quality was confirmed to have an industry standard leak rate of less than 2.0 in Hg (6.77 kPa) over 5 minutes. Temperatures profiles were monitored with thermocouples placed in the layup. A pressure of 85 psi (586 kPa) was applied. Caul plates were used for even compaction during curing.

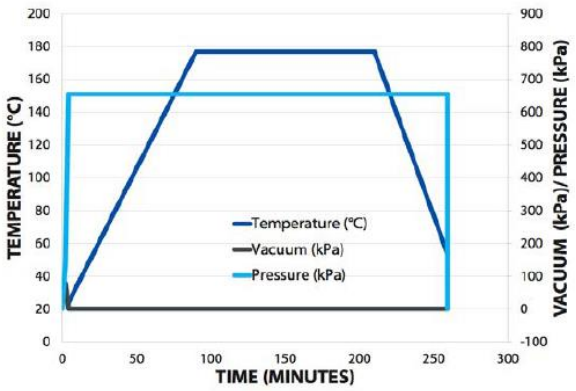

Figure 2.10: Cure cycle temperature and pressure [27]

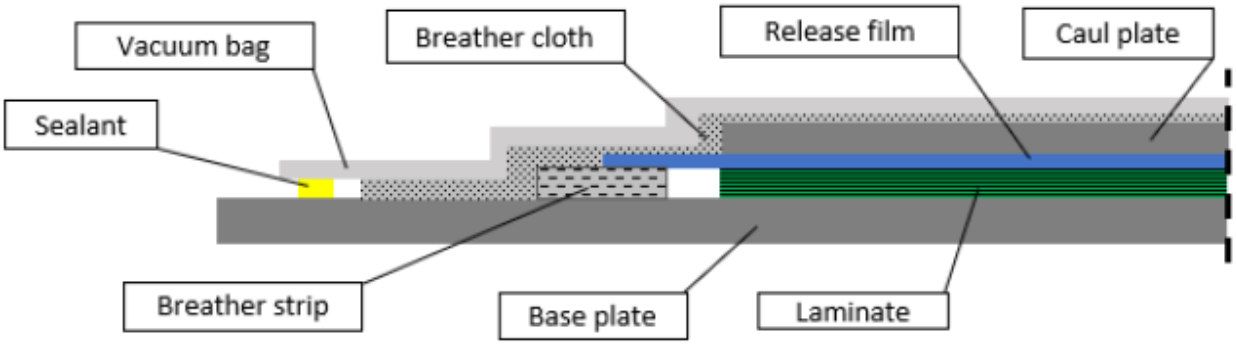

Figure 2.11: Bagging process

2.3.2 Visual and non-destructive inspections for quality control

During manufacturing, defects were manually embedded as described in section 3.1. After specimen cutting, for quality control, 5 randomly chosen coupons of different configurations were analyzed using non-destructive inspection techniques (NDI). Figure 2.12 shows pictures from the thermographic inspection, where defects are highlighted using red circles. Figure 2.13 shows similar results from the ultrasonic tests.

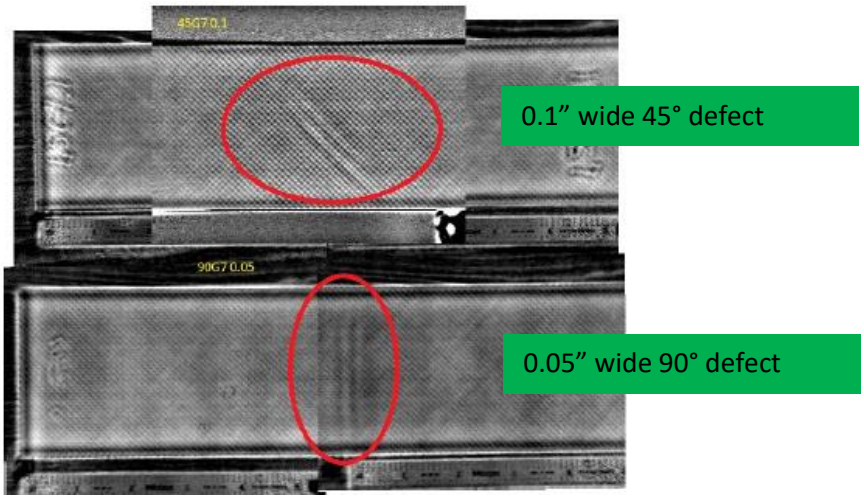

Figure 2.12: Thermographic inspection of two different coupons (each coupon is 3”, 7.6 cm wide)

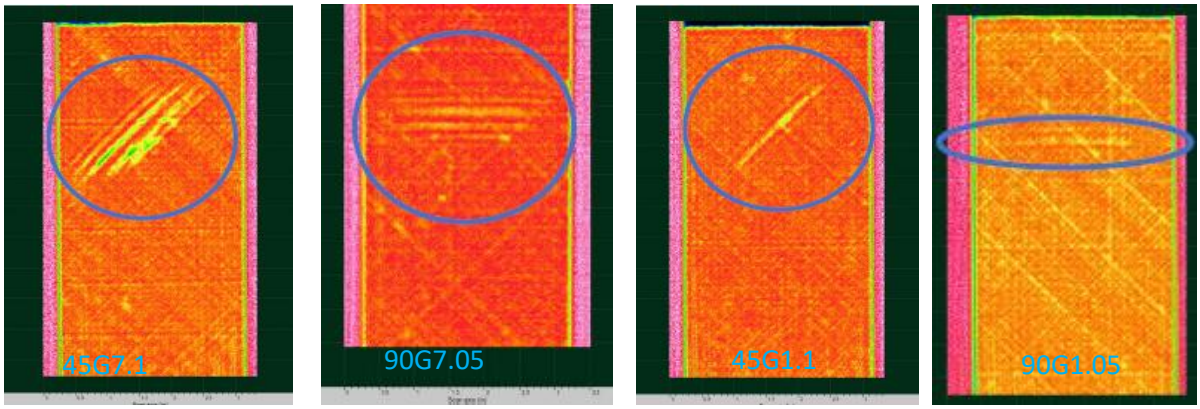

Figure 2.13: Images from the ultrasonic technique with marked defects (each coupon is 3”, 7.6 cm wide)

These non-destructive inspection techniques provided a measure of quality control on the coupon manufacturing.

2.4 Microscopy analysis: change in defect dimensions post cure

Microscopy analysis was conducted to study the effect of curing on the defects present in carbon-epoxy laminates and to see the exact geometry of defects post cure. The results of this analysis are critical for modeling the mechanical performance of specimens. The finite element models are discussed in detail in part 2 of this two-part paper [29]. This section focuses on analysing micrographs of the coupons.

For clarity and conciseness, we refer to defects in 0° plies as 0° defect, defects in 45° plies as 45° defect and so on. A single coupon contained either 0° defect(s), 45° defect(s) or 90° defect(s) exclusively (except for coupons labelled “Mix”, which contained a combination of defects). For “Mix” coupons, four defects were embedded in plies of different orientation, namely 0°, -45°, 45° and 90°.

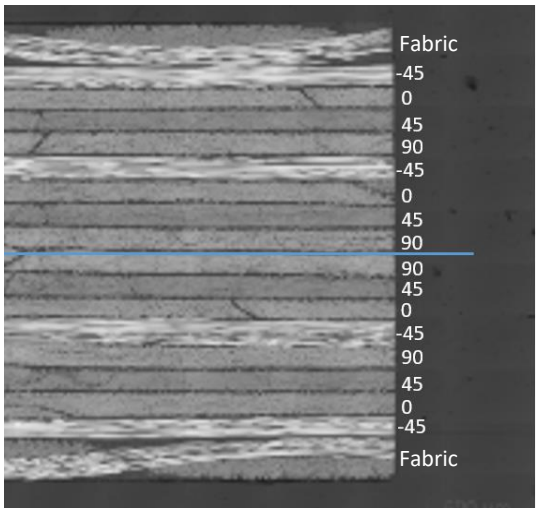

Figure 2.14: Orientation of plies in coupons used for experiments. The blue horizontal line indicates plane of symmetry.

Defect parameters (orientation, number and size of defect) were varied to generate 17 different defect configurations. These coupons are listed in the table 2.2 below along with their naming convention.

Table 2.2: List of 17 coupon configurations used for microscopy. Note the naming convention: (defect angle)G(# of defects).(defect length)

Coupon	Defect orientation	Number of defects	Size of defects, in (mm)
0G3.1	0°	3	0.1 (2.54)
0G4.1	0°	4	0.1 (2.54)
0G4.05	0°	4	0.05 (1.27)
0G7.1	0°	7	0.1 (2.54)
0G7.05	0°	7	0.05 (1.27)
45G1.1	45°	1	0.1 (2.54)
45G3.1	45°	3	0.1 (2.54)
45G4.1	45°	4	0.1 (2.54)
45G4.05	45°	4	0.05 (1.27)
45G7.1	45°	7	0.1 (2.54)
45G7.05	45°	7	0.05 (1.27)
45G10.05	45°	10	0.05 (1.27)
90G1.05	90°	1	0.05 (1.27)
90G3.05	90°	3	0.05 (1.27)
90G4.05	90°	4	0.05 (1.27)
90G7.05	90°	7	0.05 (1.27)
MixG4.05	Mix (0°, -45°, 45°, 90°)	4	0.05 (1.27)

Each specimen was cut at three different locations transverse to the embedded defects, as shown in Figure 2.15. Two cross sections are at the beginning and end of the defects and one cross section is at the middle where the defect is the widest. The cross sections on the sides of the defect are located approximately one-third of the defect length away from its middle position relative to a

perfectly manufactured defect. Thus, the analysis of these side cross-sections will give qualitative information on the healing of the defect (modification of the defect during curing due to shear flow) and its final length. If no defect is observed on the sides but it is observed at the middle cross section, it can be concluded that the defect partly healed on the sides to finally disappear during the cure cycle.

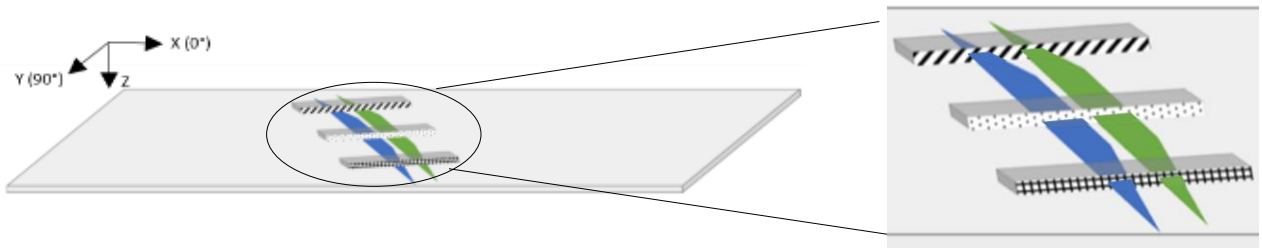

(a)

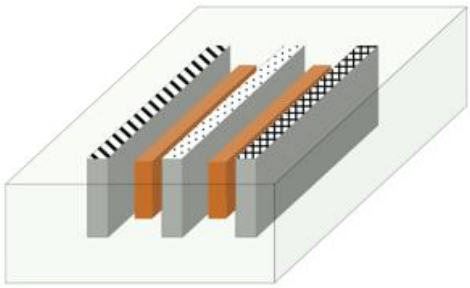

(b)

Figure 2.15: (a) Defect and the location of cut sections. (b) Placing the 3 different sample sections (indicated by different shading patterns) in epoxy puck for microscopy. The brown objects indicate spacers.

The microscopy samples were cast in epoxy and polished in a series of steps until a mirror surface finish was obtained. The polished surfaces were observed using a Nikon Eclipse L150 microscope with automated stage and bright light illumination.

Before the cure, gap and overlap have the same width. Microscopy analysis gave interesting insights into the changes in defect geometry due to curing. In general, the length of the gap decreased and the length of the overlap increased. Apart from these observations, two new intermediate regions were created from overlap to gap and from defect-free ply to gap. We will refer to these regions as "Flow". The Flow regions correspond to resin and fibre filling in the gaps due to shear flow during curing. These two regions correspond to a gradient from high fibre content in overlaps to low fibre content in gaps. Out-of-plane fibre waviness occurs as fibres from adjacent plies fill in the gaps. A typical microscopy image of a 45° defect post cure with demarcated regions is shown in Figure 2.16.

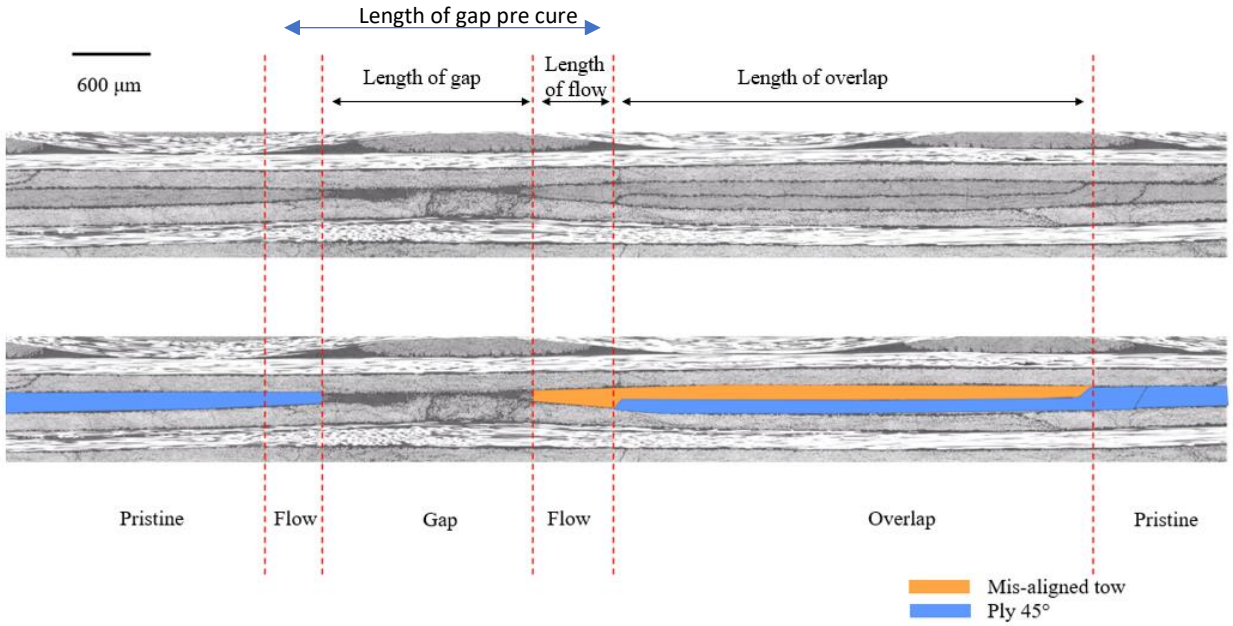

Figure 2.16: Microscopy regions of 45° defect showing different regions (top) and the same regions highlighted (bottom).

The size of the defect (gap or overlap) at the center of the Figure 2.16 coupon pre-cure was known to be 0.1 in (2.54 mm). After curing, the length of the gap, overlap and flow were measured from microscopy images (these post-cure lengths are described in Figure 2.16, along with the approximate location of the original pre-cure length).

Based on the 17 coupons used for microscopy, gaps shrank by 36% and overlaps increased by 23%, on average. Microscopy mosaics were analyzed using ImageJ software following the image analysis technique found in Mil-Handbook-17 [30]. Thresholds were applied to convert pictures to grey-scale images: resin, voids, foreign bodies and fibres were visualized with different grey tones and the number of pixels of each color were counted by ImageJ to give the fibre volume fraction in different regions of the post cure defect. Average fibre volume fraction in gap regions was 39%, while it was 67% in overlap regions and 58% in flow regions. Fibre volume fraction of defect-free plies was 64%. Further, certain trends were monitored between configurations and dimensions of defects. Length of the flow increased with the number of defects, as shown in Figure 2.17. This could be a result of increased movement due to the presence of more defects.

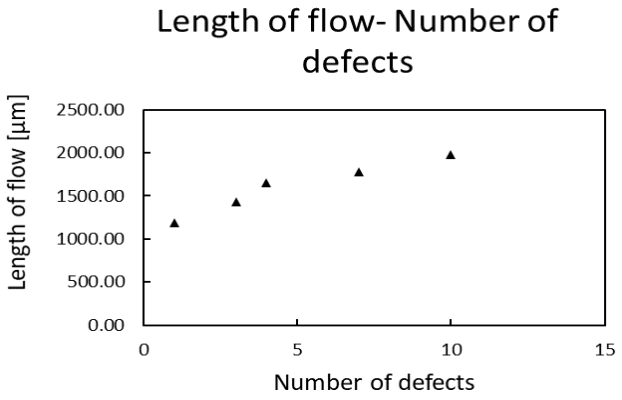

Figure 2.17: Length of flow vs number of defects

The maximum ply out-of-plane waviness increased slightly with the number of defects (marginal effect as shown in Figure 2.18 a) while the percentage of defects completely healed/covered post cure (i.e. with zero gap) decreased almost linearly with the number of defects (Figure 2.18 b).

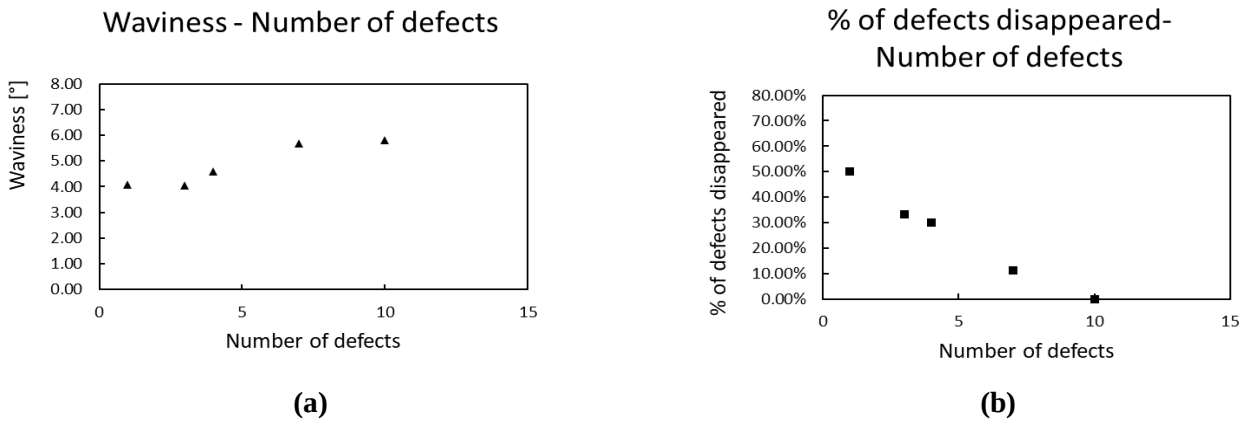

(a) **(b)**

Figure 2.18: Trends between (a) maximum ply waviness and (b) completely healed defects vs number of defects

Although this appears to contradict Figure 2.17, the explanation is likely that fewer defects will completely heal when there is a large number of defects. The fibre volume fractions in all the regions (gap, overlap and flow regions) could not be reliably related to the number, orientation and size of defects. The maximum ply waviness, which highly depends on the ply layup sequence and defect configuration, was on average, 7° for 45° defects, 6° for 0° defects and 3° for 90° defects.

The mixed orientation MixG4.05 configuration is difficult to analyze because the cross sections were transverse to some of the defects. Since 4 different orientations are present in MixG4.05, the cross sections were made at -45° to see +45° defect. No defect was visible on any of the three cross sections of MixG4.05, as shown in Figure 2.19 (defects were either healed or missed). The

micrographs revealed an organized mesostructure without waviness, with only a few small overlaps at the middle cross section.

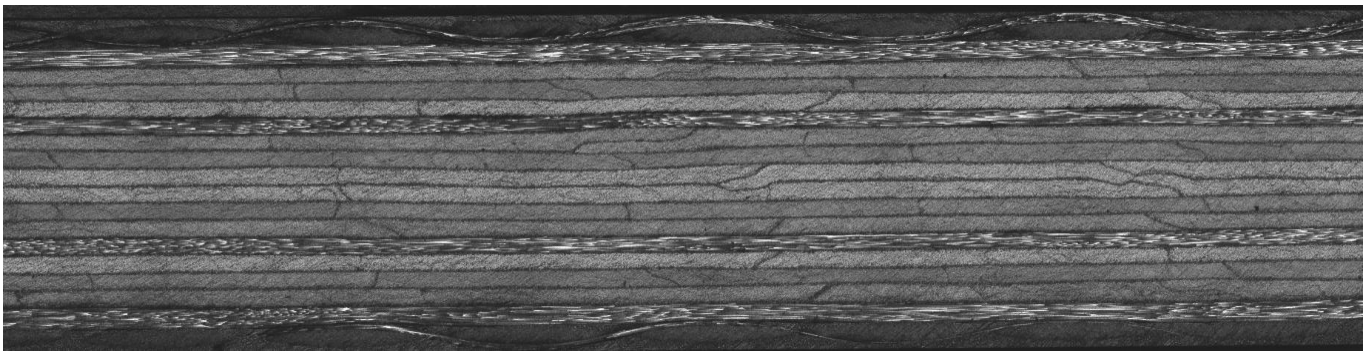

Figure 2.19: Microscopy image of Mix defect configuration

A typical 90° coupon is used here to illustrate the result of healing (Figure 2.20). For all 90° coupons, the cross sections were made at 0° along the length of the specimen. None of the micrographs showed any gaps at the tips. In the middle section, gaps were completely covered for 90G1.05 (shown in Figure 2.20).

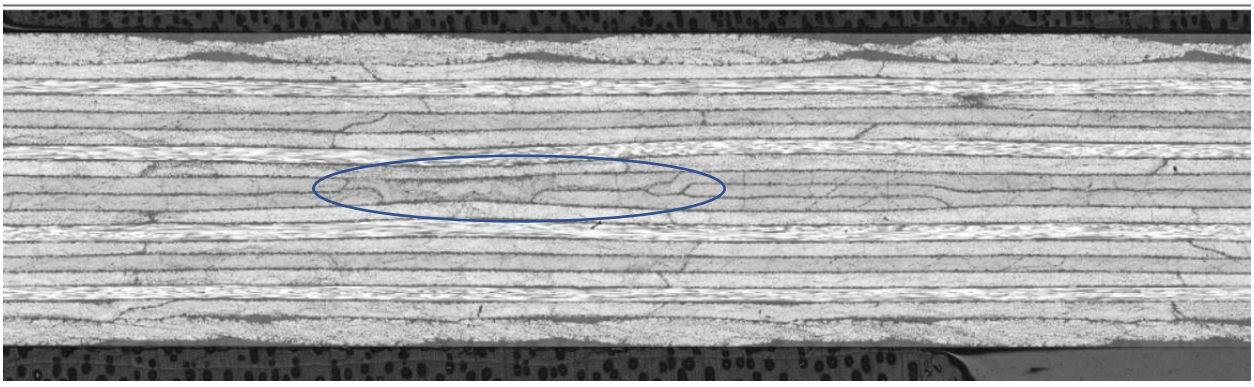

Figure 2.20: Healed gap of 90G1.05 marked by the blue circle. Note that healing does not eliminate fibre waviness.

Small gaps of the order of 100 microns were visible in 90G3.05 and 90G4.05 configurations, demonstrating high healing potential for 90° defects. Note that in these 90° defect configurations, two 90° defects are adjacent above and below the laminate centerline which possibly influences the ability to heal. Overlaps were visible in the middle sections of all 90° defects. Configurations 45G3.1 and 45G7.1 both show all half gap / half defects that were embedded during the manufacturing of coupons. While the middle cross sections – Figure 2.21 and Figure 2.22 – show the right number of defects at their expected locations, not all the defects appear on the side cross sections. Side cross section shown in Figure 2.23 of the configuration 45G7.1 shows 2 half gap / half overlap defects out of 7 while none were visible for 45G3.1 (micrographs not shown because the laminate mesostructure is defect-free). Since defects are visible primarily in the middle cross sections but not always on the side cross sections, it seems that defects have healed due to shear flow of fibres and resin during the cure cycle (in addition, adjacent plies above and below tend to fill up part of the gap, causing waviness). It appears that defects smaller than 0.05 in (1.27 mm) wide at least partially healed during the cure cycle.

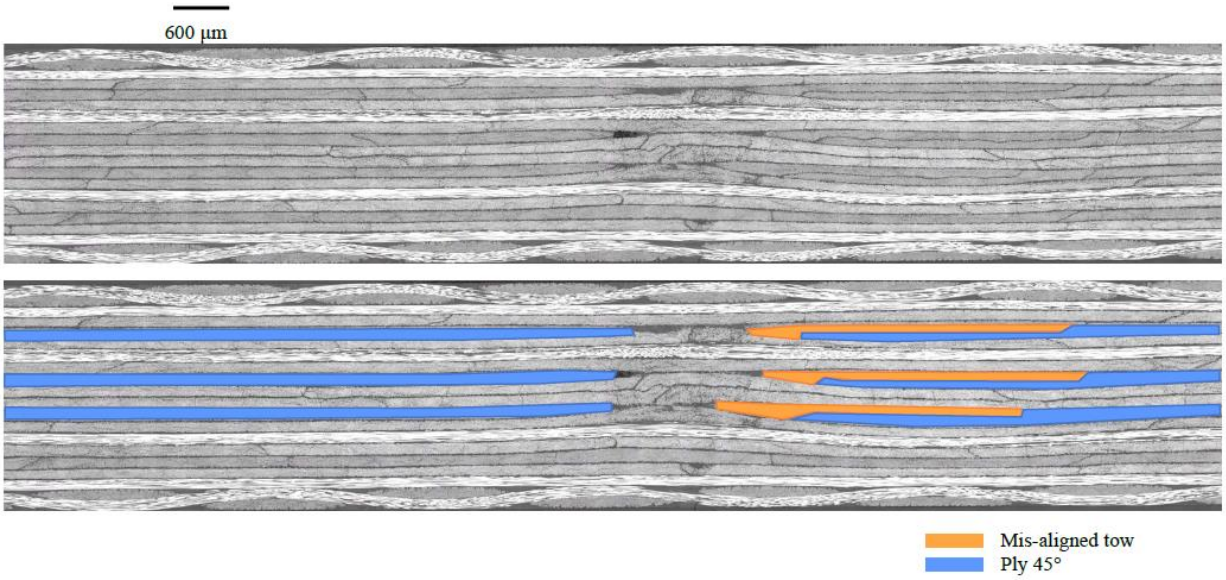

Figure 2.21: Middle cross section of 45G3.1 with highlighted defects

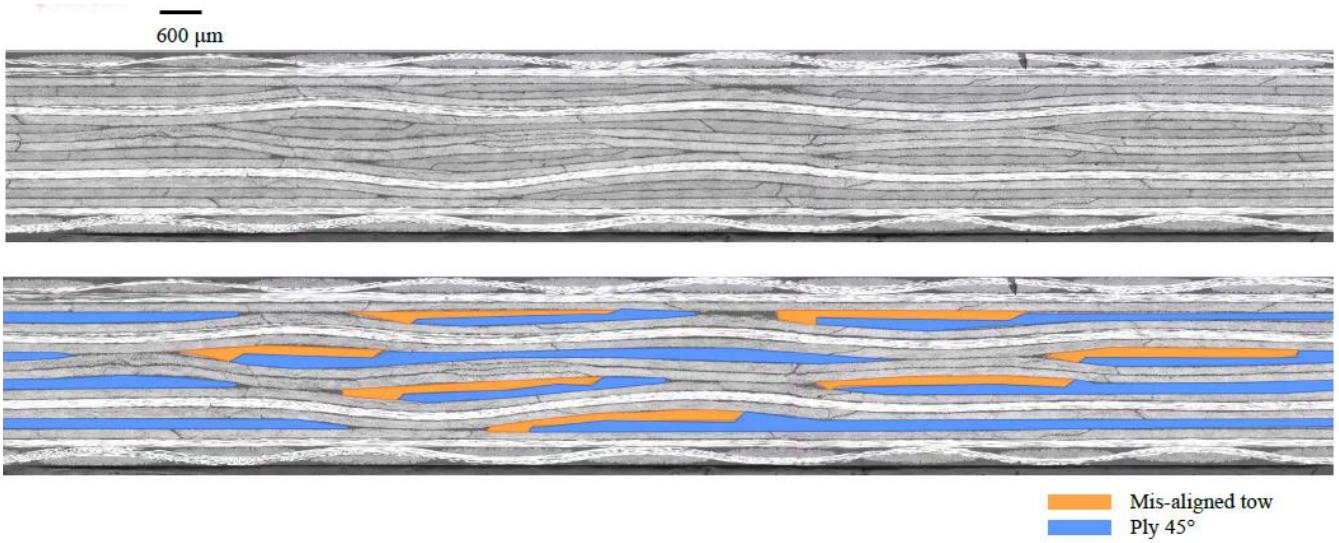

Figure 2.22: Middle cross section of 45G7.1 with highlighted defects

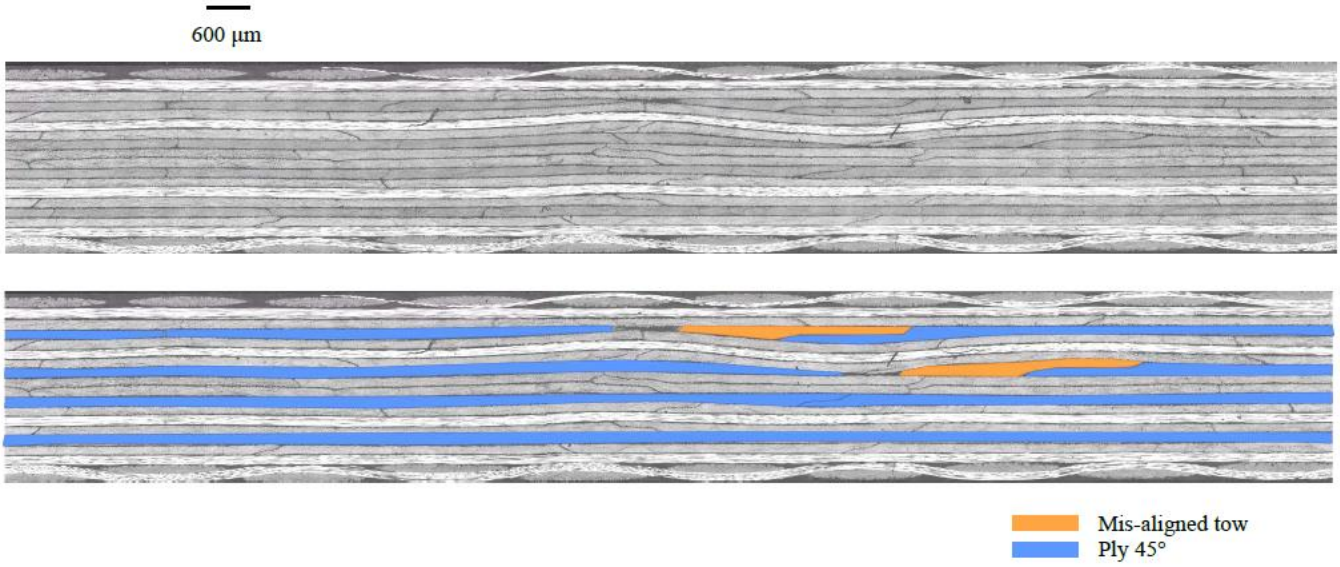

Figure 2.23: Side cross section of 45G7.1 with marked defects, indicating that 5 defects out of 7 have probably healed at this location

The microscopy results explained in this section have been used to inspire simulation models to model the performance of laminates (refer paper 2 [29]).

2.5 Experimental setup and results

2.5.1 Tension test methodology and results

Tensile tests were performed following ASTM D3039 [24]. Coupons were set up for loading in an MTS machine of 250 kN maximum load capacity. For each coupon, the thickness and width were measured at both ends and in the middle in order to calculate the cross-section area and then the engineering stress. One end of the coupon was kept fixed and the other was loaded using displacement control at a rate of 2 mm/sec. The load and displacement were recorded during the experiments, which automatically stopped when the load dropped by at least 50% due to catastrophic failure.

The fracture path of the coupons was observed in 45° or 90° plies, independent of the defect configuration of the specimen. Five coupons were tested per defect configuration, but no pattern would emerge as to the final fracture mechanism because most of the coupons failed catastrophically for the tensile tests.

For strain measurement, a few coupons were tested with an extensometer installed and others using Digital Image Correlation (DIC). The stress vs strain curves normalized with respect to defect-free performance is shown in Figure 2.24.

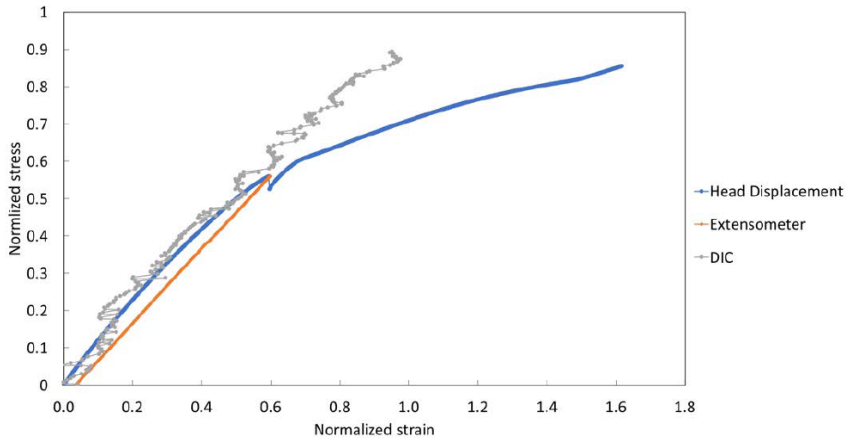

Figure 2.24: Configuration 90G7.05: stress strain curves normalized with respect to defect-free performance

The extensometer has to be removed before the coupon fails otherwise it could be damaged during coupon failure. The extensometer was removed at half the predicted failure load to increase the safety of this operation. Referring to figure 2.24, despite being noisy data, the DIC stress strain curve results correlate well with the extensometer measurement and no non-linearity is observed in the elastic region. The DIC is observable till the final fracture of the specimen. It is suspected that the non-linearity of the head displacement is due slipping of the aluminium tabs that were used to ensure that the MTS grips were safely gripping the coupons. Thus, there was a need to measure displacement using DIC and/or extensometer. The average laminate modulus measured with either the extensometer method or the DIC method is within 10% of the theoretical modulus by classical laminate plate theory.

Compared to laminate theory, defect-free coupons failed at a maximum stress 9% lower than the expected theoretical value in tension, perhaps due to edge effects. Before the fracture, all coupons, even the defect-free configuration, experienced wide delamination between the 9th and 10th plies which are oriented at 90°. Each specimen opened from the middle toward the grips in such way

that it was possible to see through the coupons. Grips of the MTS machine prevented further delamination. This damaged structure was able to carry more load with the support of the MTS grips. However, the tests were kept running until failure. It is not clear whether the delamination started on the edge or in the middle. Note that DIC only shows the deformation on the outer surface so it is impossible to see how much delamination there is through-the-thickness using this technique. No correlation between the orientation of defects and high strain regions can be made. The fracture mechanism for the different configurations could be highly influenced by a progressive delamination in the vicinity of defects without any certainty that defects played a specific role.

The results for the various configurations of defects are plotted in Figure 2.25 for 0.1 in (2.54 mm) wide defects configurations and in Figure 2.26 for 0.05 in (1.27 mm) wide defect configurations. Their corresponding coefficient of variation is calculated. Each data point is the average normalized max stress of 5 coupons of the same configuration.

$$COV = \frac{\sqrt{\frac{\sum_{i=1}^{N}\left(x_i - x_{avg}\right)^2}{N-1}}}{x_{avg}} \qquad 2.1$$

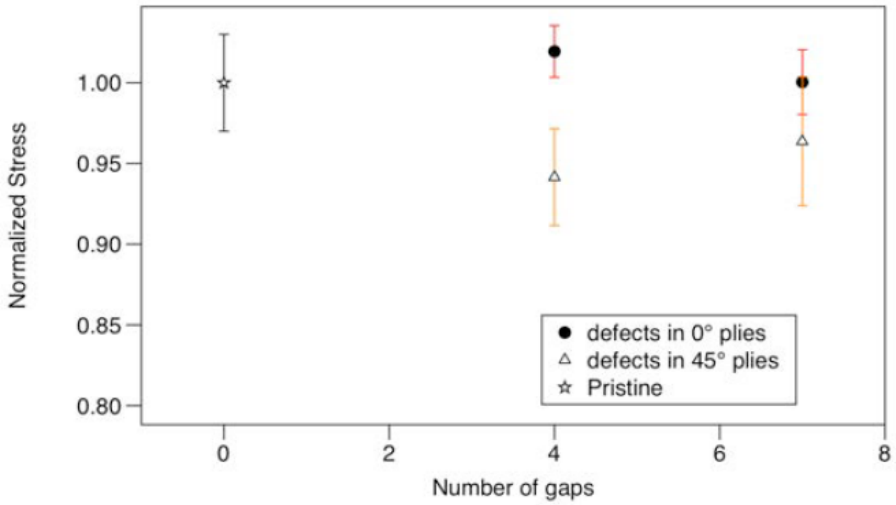

Figure 2.25: Tensile test results. Normalized stress for 0.1 in (2.45 mm) wide defect

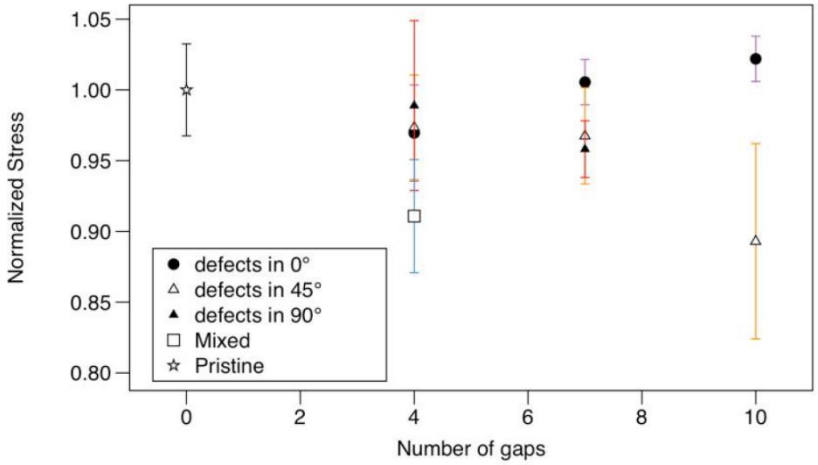

Figure 2.26: Tensile test results. Normalized stress for 0.05 in (1.27 mm) wide defect

Most of the configurations have a coefficient of variation smaller than 5%. Only 90G4.05 and 45G10.05 configurations have higher coefficient of variation, 6.2% and 6.8%, respectively.

The mixed defect orientation configuration MixG4.05 shows the largest strength reduction (9%) for 4 defects. Mix defect configuration was expected to be the worst scenario. However, the

reduction is up to 11% for 45G10.05, which also has the largest scatter while 45G7.1 was found to be slightly stronger than 45G4.1 in tension (4% and 6% strength reduction). The effect of number of defects is not clear for 45° defected coupons.

Considering 0.05 in (1.27 mm) wide defects, 90° and 45° oriented defects configurations show similar trends: the more defects, the larger the strength reductions. 45G4.05 and 45G7.05 have closer strength reductions than their wider equivalents, so the effect of size is not clear.

Results for 0° oriented defects show almost no effect on the maximum stress of coupons with an average strength reduction of 1% for both sizes. It appears that the defect size variation between 0.1 in (2.54 mm) and 0.05 in (1.27 mm) does not have much influence on coupon strength.

2.5.2 Summary of tension test results

In general, tensile experimental results show a limited effect of embedded defects on the maximum strength of tested coupons compared to the defect-free configuration. Strength reductions are usually smaller than 5% except for the case of mixed gap orientation and 45G10.05,. Coupons with 45° and 90° oriented defect configurations behave similarly and their coupons' maximum strength decreases when the number of defects increases, while 0° oriented defect configurations show almost no effects. Experimentally, it looks like defects have more effects when they are loaded in the matrix direction. This can be attributed to waviness which is more pronounced in 0° plies when 90° and 45° have defects. This means configurations that induced more waviness in 0° plies show the highest strength reductions. Matrix cracking and delamination might be the initiators of the fracture propagation.

2.5.3 Compression test methodology and results

Compression tests were performed following ASTM D6484 [25]. Coupons were installed in the compression fixture with anti-buckling devices according to the standard. Two sizes of fixtures were used corresponding to the two sizes of coupons: 1.5 in (38.1 mm) and 3 in (76.2 mm) wide.

Stress strain curves obtained in compression from cross-head displacement curves show, for all coupons, only a slightly non-linear behaviour, as shown in Figure 2.27. A mark placed on the side of the coupons confirms that there was no slip inside the fixture. No tests were performed with an extensometer because there was no room to install one on a coupon due to the large size of the fixture of ASTM D6484 [25], as shown in Figure 2.5.

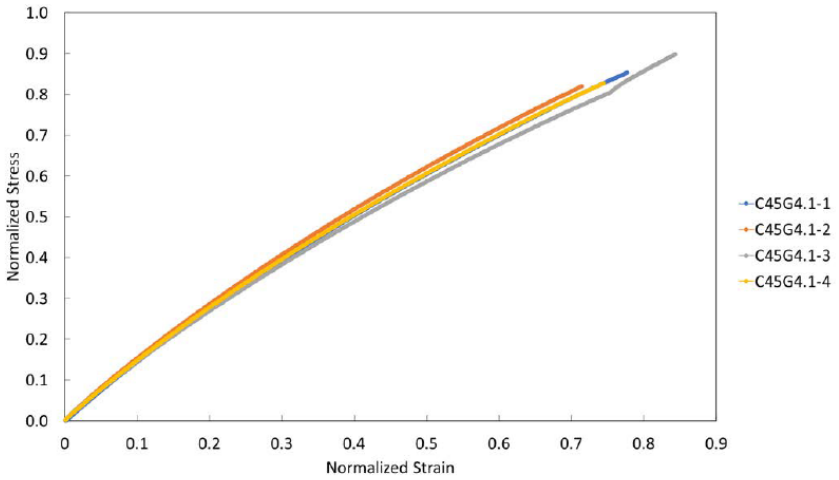

Figure 2.27: C45G4.1 stress strain curves using head displacement measurement.

For clear cases of failure at the middle of the specimen, the crack path is at 45° through-the-thickness as shown in Figure 2.28, which is characteristic of compression for quasi-isotropic laminate failure.

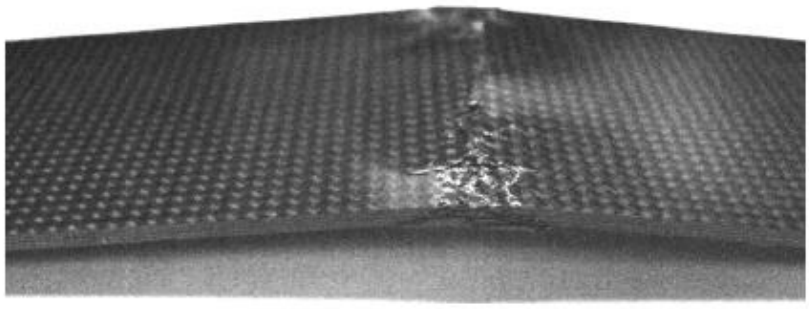

Figure 2.28: Failure in the region of the middle of the window of the fixture

2.5.4 Summary of compression test results

The strength reductions obtained for compressive tests are much larger than those obtained from the tensile tests of section 5.1. The 45° and 90° configurations behave similarly, see Figure 2.29: the more defects, the lower the strength. The scatter also increases with the number of defects. Generally, the coefficient of variation is close to 5% with the exception of 45G10.05, which reaches 16% and 45G7.1, which reaches 9%. The 45° oriented defect configurations plotted in Figure 2.30 have a strength reduction that goes from 20% for 4 defects to 25% for 10 defects. The 90° oriented defects configurations are less than 5% stronger for the same number of defects than 45° defects. Mixed orientation defects configurations have the largest strength reduction with only 4 defects, at 28% strength reduction. If more defects had been introduced in mixed orientation it is expected that larger strength reductions would have been obtained.

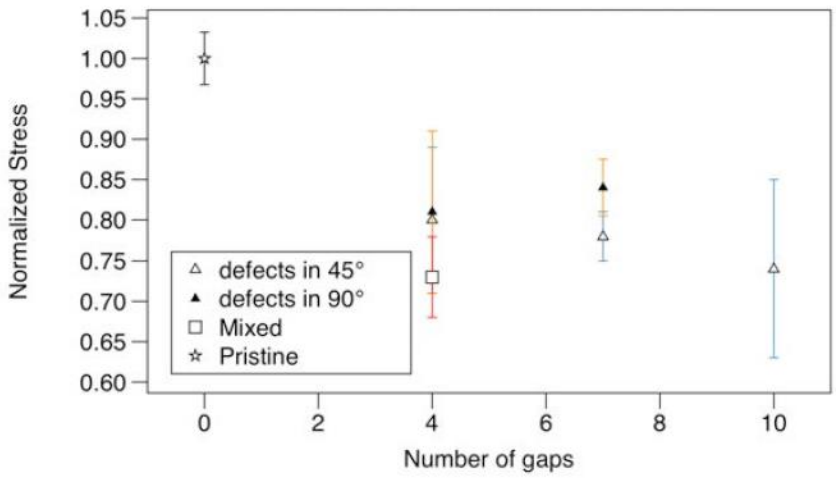

Figure 2.29: Compression normalized stress at failure - Defects 0.05in (1.27mm) wide

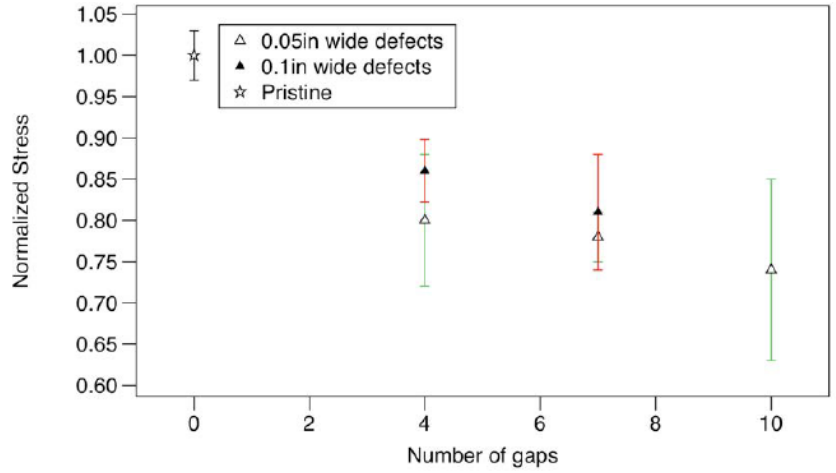

Figure 2.30: Compression normalized stress at failure - Defects 45° oriented

As has been mentioned by Wisnom et al. [31], fibre waviness should play an important part in failure of AFP materials with defects. Compression loading is examined here since tensile tests usually had much smaller strength reductions. Figure 2.31 shows a graph of all compression test failure levels and measured fibre waviness. Although there is no distinct pattern in Figure 2.31, one can see that there is a possible influence of waviness in the results. For measured waviness

greater than about 5°, some samples have large reductions in strength, which does not occur as much when waviness is around 4° or less. However, note that there are not enough samples to make a statistically accurate assessment of the influence of fibre waviness.

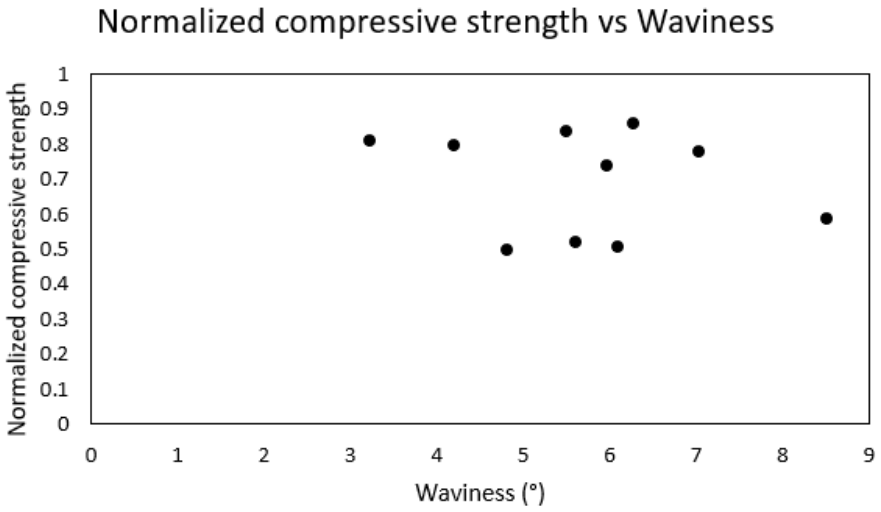

Figure 2.31: Compression normalized stress vs waviness

2.5.5 Fatigue test fixture setup and methodology

During the fatigue life of a specimen, damage accumulates due to repetitive load application in tension and compression. For industrial applications, the knowledge of the mechanical performance of composite structures under fatigue loading is essential to design safe vehicles with a long life. The single application of any load (maximum load of the cycle) would not damage the material because the load magnitude is far below the quasi-static maximum stress. Since composite laminates in this study are manufactured with intrinsic acceptable flaws, the laws of fatigue life probably differ from those defined for defect-free structures.

Fatigue tests were performed with the same MTS loading machine and the same fixtures that have been used for compression. ASTM D6484 [25] describes loading conditions that have been

followed for cycles of tension and compression with stress ratio r = −1, which means the magnitude of tension load equals the magnitude of compression load (otherwise known as “fully reversed loading”). The loading curve is a sine wave at a frequency of 5Hz. The frequency is an important parameter because if it is too high, the friction in the fixture and in the laminate can increase the temperature thus degrading the material properties too fast. A very low frequency is better to avoid these unwanted dynamic effects and sudden energy release, but testing time is much longer. In the literature, a frequency of 8Hz has been used [32]. The decision to use 5Hz was made because delamination appeared very fast at the beginning of the tests, in the first few cycles. A thermocouple in contact with the specimen kept track of the temperature. No coupons exceeded 32°C, which is low compared to the glass transition temperature of the epoxy 3900-2 [27]. Thus, thermal effects of matrix degradation were avoided.

One S-N curve per configuration is obtained. Nine coupons per configuration have been manufactured. Different load magnitudes are applied leading to different fatigue lives. All coupons, even defect free coupons, experienced early delamination between the 9th and the 10th plies, exactly as observed in tension tests. However, the coupons could still carry load and delamination was not considered a final failure mode. This delamination begins at the middle of the coupons and grows toward the grips. Delamination growth stops because of the pressure of the grips on the coupons. Without the grips, it is expected that coupons would have failed earlier.

All coupons failed in the expected gauge section, at their middle where defects are located. The two fixtures of different sizes were used with shims. The fracture of all coupons occurred in compression and the typical failure mode looked like Figure 2.28. In the following figures, stress

has been normalized using the maximum compression stress measured in the defect-free configuration. Figure 2.32 shows all results for all configurations in fatigue, at different applied load levels. The S-N curves follow a linear law between the applied stress and the logarithm of number of cycles. Life between 1000 cycles and 1,000,000 cycles were targeted during testing.

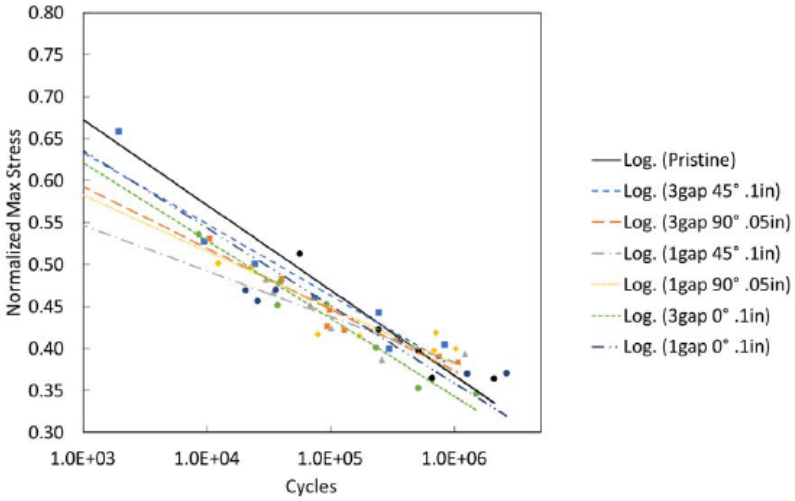

Figure 2.32: S-N curves of all configurations

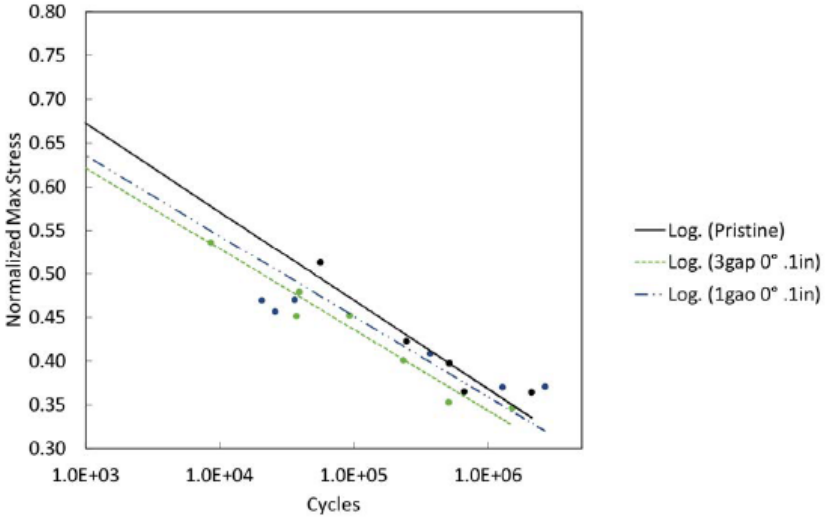

Figure 2.33: 0° configuration S-N curves

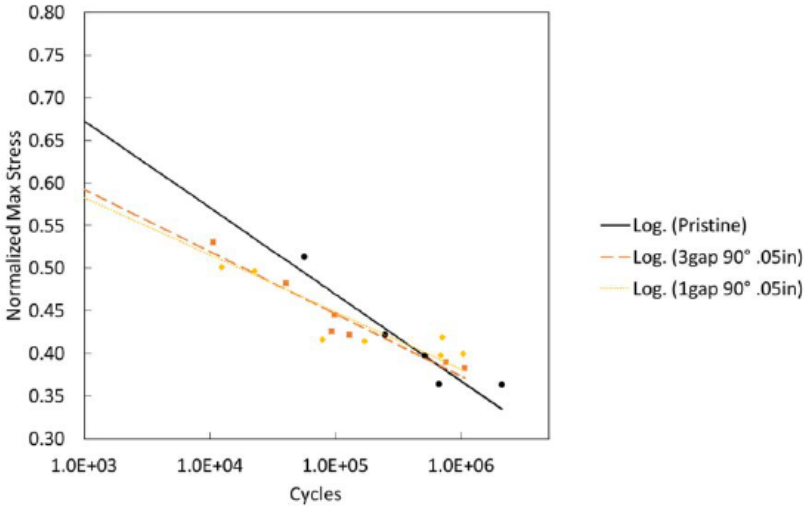

Figure 2.34: 90° configuration S-N curves

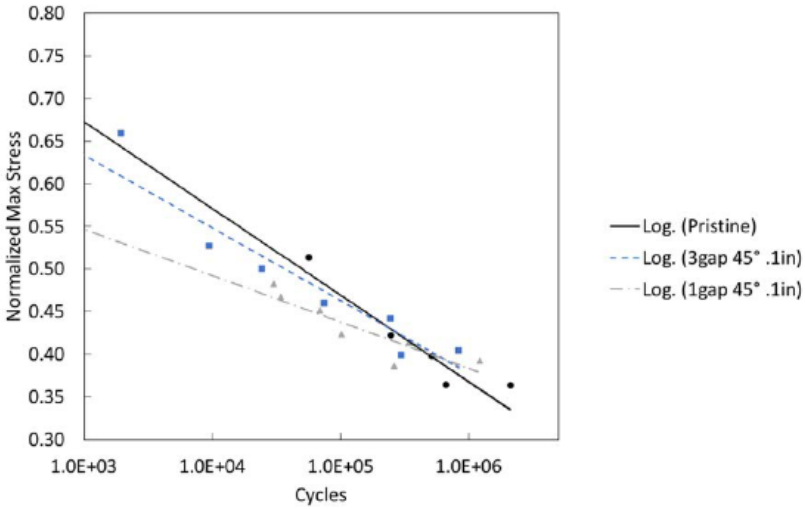

Figure 2.35: 45° configuration S-N curves

Defects appear to have more effect on fatigue life at higher stresses. The 0.05 in (1.27 mm) wide defects are among the configurations with largest strength reductions while other configurations with 0.1 in (2.54 mm) wide defects tend to resist better.

There is a threshold of applied stress below which the effects of defects are close to the defect-free configuration. At about 40% of the pristine load and one million cycles, the defected configurations behave like pristine coupons.

Figure 2.33, Figure 2.34 and Figure 2.35 emphasize the effect of the number of defects in one orientation and one size. 0° and 90° oriented defects show the same trends for both 1-defect and 3-defects configurations while 45° oriented defects configurations present the two extremes of all the fatigue results: 45G1.1 is extremely close to the defect-free configuration even at high stresses while 45G3.1 leads to the largest strength reduction factors at high stresses.

2.5.6 Discussion of results from fatigue tests

It was found that at low stress levels the tendency of the material to propagate damage from embedded defects is low, which is good news for lightly loaded structures. The mechanical behavior is close to defect-free coupons under a certain load threshold estimated at 40% of maximum compression quasi static strength. This stress threshold corresponds to fatigue lives of more than 1,000,000 cycles.

Since displacement measurements were made using the cross-head displacement of the MTS machine, no stiffness analysis was attempted. It is expected that non-linearity in stress strain behavior is the result of both matrix cracking and delamination. Specimen collapse is due to fibre breakage according to fracture observations. Early delamination could weaken the laminate. It was found that delamination typically occurred between two 90° plies. Thus, the choice of stacking

sequence can have an impact on fatigue life of coupons. Out-of-plane waviness is an expected cause of failure degradation, as relevant in fatigue as it was in tension and compression.

2.6 Conclusion

Automated Fibre Placement technology enables efficient manufacturing of large complex panels, increasing the yield and decreasing material waste. However, this manufacturing process has its own induced defects. This research was interested in the effects under tension, compression and fatigue of side-to-side half gap / half overlap defects. The influence of several defect parameters was studied in detail. Coupons of different configurations with varying size, pattern and orientation of embedded defects have been manufactured and tested. From test results, it is suggested that both out-of-plane waviness and the healing process of closing gaps between tows during curing (with caul plates) play a major role on the effect of defects. Healing due to the movement of both fibres and resin under compaction (shear flow) depends on the stacking sequence and on the plies in which defects are embedded. Increasing the defect width does not necessarily decreases the maximum strength further.

Compression is more critical than tension and the largest strength reductions reached 25% compared to 10%, respectively. However, these results correspond to worst case scenario configurations that would likely not be acceptable in the manufacturing of flightworthy parts. In general, the tension average strength reduction is about 5% and the compression average strength reduction is close to 20% for all configurations. The 45° and 90° configurations behave similarly in both compression and tension: their strength decreases more when the number of defects increases. Limited testing of mixed defect orientation configurations have even worse performance

but this would have to be confirmed with further tests. In fatigue, configurations have been tested under tension-compression R = −1. Defected configurations have larger strength reductions at high stresses but a threshold exists under which their performance is very close to the defect-free configuration. The 45° configurations are very sensitive to the number of defects while it does not appear to have any effect on 90° configurations.

It is suspected that the stacking sequence, therefore the position through-the-thickness of each ply orientation, might have an effect on the magnitude of waviness and healing of embedded defects. The certification of composite structures manufactured with AFP requires an understanding of the failure mechanism of the laminates too. In tension and fatigue, delamination propagates along the defects toward the edges, leading to matrix cracking in 90° and 45° plies. Without the support of the grips during testing, it is expected that laminates had failed earlier. However, due to the presence of the grips to prevent further delamination, coupons were still able to carry load. The final failure is due to fibre breakage in 0° plies which carry most of the load in both tension and compression**.**

This work provides a good set of tests for AFP-manufactured materials, examining both the intrinsic behaviour of the defects themselves and their effects of the strength of coupons containing the defects, under tension, compression and fatigue loading. It is clear that many other defect configurations could be examined in the future, depending on what a manufacturer expects to see in produced parts.

2.7 Acknowledgements

This research project was done in collaboration with our funding partners, Bell Textron Canada Limited and National Research Council, Aerospace Manufacturing Technology Centre (NRC-AMTC). Funding from the Natural Science and Engineering Research Council of Canada (NSERC) is gratefully acknowledged, as well as cooperation from Center for Research on Polymers and Composites (CREPEC).

References

1. Lukaszewicz, D.H.J.A., C. Ward, and K.D. Potter. *The engineering aspects of automated prepreg layup: History, present and future*. Composites Part B: Engineering, 2012. 43(3): p. 997-1009.
2. Chen, J., et al. *Manufacturing of composite helicopter tailboom using afp process.* in 70th American Helicopter Society International Annual Forum 2014, May 20 - 22, 2014, Montreal, QC, Canada: American Helicopter Society.
3. Abdi, F., et al. *Certification modeling of composites fuselage, considering effect of defects from fiber placement manufacturing processes*. in 55th AIAA Aerospace Sciences Meeting, January 9 - 13, 2017, Grapevine, TX, United states: American Institute of Aeronautics and Astronautics Inc.
4. Juarez, P.D., K.E. Cramer, and J.P. Seebo. *Advances in in situ inspection of automated fiber placement systems.* in Thermosense: Thermal Infrared Applications XXXVIII, April 18-21, 2016, Baltimore, MD, United states: SPIE.
5. *SA2GE Project*. in *Composite Fuselage Structures*. 2015, Bell Helicopter Textron Canada Limited.
6. Sawicki, A.J. and P.J. Minguet. *Effect of intraply overlaps and gaps upon the compression strength of composite laminates.* in Proceedings of the 1998 39th AIAA/ASME/ASCE/AHS/ASC Structures, Structural Dynamics, and Materials Conference and Exhibit and AIAA/ASME/AHS Adaptive Structures Forum. Part 1 (of 4), April 20 - 23, 1998, Long Beach, CA, USA: AIAA.
7. Croft, K., et al. *Experimental study of the effect of automated fiber placement induced defects on performance of composite laminates*. Composites Part A: Applied Science and Manufacturing, 2011. 42(5): p. 484-491.
8. Elsherbini, Y.M. and S.V. Hoa. *Experimental and numerical investigation of the effect of gaps on fatigue behavior of unidirectional carbon/epoxy automated fiber placement laminates.* Journal of Composite Materials, 2017. 51(6): p. 759-772.

9. Elsherbini, Y. and S.V. Hoa. *Fatigue behavior of unidirectional carbon/epoxy AFP laminates containing gaps*. in 31st Annual Technical Conference of the American Society for Composites, ASC 2016, September 19-21, 2016, Williamsburg, VA, United states: DEStech Publications Inc.
10. Turoski, LE. *Effects of Manufacturing Defects on the Strength of Toughened Carbon/Epoxy Prepreg Composites.* MSc Thesis, Montana State University, 2000.
11. Nguyen MH, Vijayachandran AA, Davidson P, Call D, Lee D, Waas AM. *Effect of automated fiber placement (AFP) manufacturing signature on mechanical performance of composite structures*. Composite Structures, 2019, 228.
12. Ghayour, M., Hojjati, M., Ganesan, R. *Effect of tow gaps on impact strength of thin composite laminates made by Automated Fiber Placement: Experimental and semi-analytical approaches*. Composite Structures, 2020, 248: p. 1-10.
13. Fayazbakhsh, K., et al. *The effect of gaps and overlaps on the in-plane stiffness and buckling load of variable stiffness laminates made by automated fiber placement.* in 15th European Conference on Composite Materials: Composites at Venice, ECCM 2012, June 24 - 28, 2012, Venice, Italy: European Conference on Composite Materials, ECCM.
14. Fayazbakhsh, K., et al. *A study of the influence of gaps and overlaps on the strength of composite panels made by automated fiber placement*. in 26th Annual Technical Conference of the American Society for Composites 2011 and the 2nd Joint US-Canada Conference on Composites, September 26 - 28, 2011, Montreal, QC, Canada.
15. Fayazbakhsh, K., et al. *Defect layer method to capture effect of gaps and overlaps in variable stiffness laminates made by Automated Fiber Placement*. Composite Structures, 2013. 97: p. 245-251.
16. Talreja, R. *FATIGUE OF COMPOSITE MATERIALS: DAMAGE MECHANISMS AND FATIGUE-LIFE DIAGRAMS*. Proceedings of The Royal Society of London, Series A: Mathematical and Physical Sciences, 1981. 378(1775): p. 461-475.

17. Kobayashi, S. and N. Takeda. *Experimental and analytical characterization of transverse cracking behavior in carbon/bismaleimide cross-ply laminates under mechanical fatigue loading.* Composites Part B: Engineering, 2002. 33(6): p. 471-478.
18. Kawai, M., et al. *High-temperature off-axis fatigue behaviour of unidirectional carbon-fiber-reinforced composites with different resin matrices*. Composites Science and Technology, 2001. 61(9): p. 1285-1302.
19. Jen, M.-H.R., et al. *Fatigue response of APC-2 composite laminates at elevated temperatures*. Composites Part B: Engineering, 2008. 39(7-8): p. 1142-1146.
20. Mandell, J.F. and U. Meier. E*ffects of Stress Ratio, Frequency, and Loading Time on the Tensile Fatigue of Glass-Reinforced Epoxy.* in Long-Term Behavior of Composites, Symposium, 1983, Williamsburg, VA, USA:ASTM.
21. Colombo, C. and L. Vergani. *Influence of delamination on fatigue properties of a fibreglass composite.* Composite Structures, 2014. 107(1): p. 325-333.
22. Maragoni, L., Modenato, G., De Rossi, N., Vescovi, L. and Quaresimi, M. *Effect of fibre waviness on the compressive fatigue behavior of woven caron/epoxy laminates.* Composites Part B: Engineering, 2020. 199: p. 1-10.
23. Thor, M., G.R. Sause, M. and Hinterholtz, R. *Mechanisms of Origins and Classification of Out-Of-Plane Fiber Waviness in Composite Materials – A Review*. Journal of Composite Science, 2020. 130: p. 1-39.
24. *ASTM D3039*. in *Standard Test Method for Tensile Properties of Polymer Matrix Composite Materials*. 2014, West Conshohocken, PA: American Society for Testing and Materials.
25. *ASTM D6484*. in *Standard Test Method for Open-Hole Compressive Strength of Polymer Matrix Composite Laminates*. 2014, American Society for Testing and Materials: West Conshohocken, PA.

26. Lessard, L.B., A.S. Schmidt, and M.M. Shokrieh. *Three-dimensional stress analysis of free-edge effects in a simple composite cross-ply laminate.* International Journal of Solids and Structures, 1996. 33(15): p. 2243-2259.
27. Toray. *Resin system 3900-2*. 2019.
28. Ibrahim, M.E. *Nondestructive evaluation of thick-section composites and sandwich structures: A review.* Composites Part A: Applied Science and Manufacturing, 2014. 64: p. 36-48.
29. Cadran V., Del Rossi D., Thakur P., Lapalme M., Lessard L. *Modeling the effect of half gap/half overlap defects on the strength of composite structures fabricated using automated fiber placement (AFP) method.* Composites Part B: Engineering, 2020 (in press).
30. *Polymer matrix composite guidelines for characterization of structural materials*. MIL-HDBK-17-1F ed., vol. 1. 2002, Washington, DC, USA: US Department of Defense.
31. Li, X., Hallett, S.R., and Wisnom, M.R. *Modelling the effect of gaps and overlaps in automated fibre placement (AFP)-manufactured laminates*. Science and Engineering of Composite Materials, 2015. 22(2): p.115-129.
32. Elsherbini, Y. *Fatigue behavior of carbon/epoxy AFP laminates containing gaps*. in Mechanical Engineering. 2017, Concordia University: Montreal.

Appendix

A.1 Brief summary of microscopy test results

Parameter	Average measured/ calculated value
Gap pre vs post cure	63.88%
Overlap pre vs post cure	123.13%
Gap fibre volume fraction	38.7%
Overlap fibre volume fraction	66.91%
Flow fibre volume fraction	58.5%

A.2 Average test results of all the samples

Please refer table 2.2 in the paper for coupon nomenclatures.

A.2.1. Coupons with 0° defect

Coupons / Parameters	0G3.1	0G4.1	0G4.05	0G7.1	0G7.05
Gap – total (µm)	1732	1816.03	683.00	1812.36	920.78
Gap pre vs. post cure (µm/ µm)	68.17%	71.50%	53.78%	71.35%	72.50%
Overlap total length (µm)	3556	3309	1469	2671	1725
Overlap pre vs. post cure (µm/ µm)	139.99%	130.27%	115.67%	105.16%	135.84%
Overlap shear flow (µm)	525	528	2048	958	1822
Overlap max thickness (µm)	226	247	244	269	233
Gap fibre volume fraction	35.78%	41.25%	37.19%	43.35%	36.96%
Overlap fibre volume fraction	65.12%	63.19%	66.95%	70.53%	64.21%
Flow fibre volume fraction	53.67%	54.07%	62.42%	61.44%	58.93%
Number of defects healed	1	2	0	0	0

A.2.2. Coupons with 45° defect

Coupons / Parameters	45G1.1	45G3.1	45G4.1	45G4.05	45G7.1	45G7.05	45G10.05
Gap – total (µm)	1983.74	1526.31	1779.26	842.67	1959.29	718.05	848.08
Gap pre vs. post cure (µm/ µm)	78.10%	60.09%	70.05%	66.35%	77.14%	56.54%	66.78%
Overlap total length (µm)	3023	3336.84	2680	1632	3149	1674	1473
Overlap pre vs. post cure (µm/ µm)	119.01%	131.37%	105.53%	128.49%	124%	131.78%	115.97%
Overlap shear flow (µm)	779	752.63	774	1944	576	1810	1915
Overlap max thickness (µm)	255	205.26	270	248	267	240	243
Gap fibre volume fraction	42.39%	37.05%	44.25%	40.44%	32%	37.59%	42.88%
Overlap fibre volume fraction	68.32%	68.76%	68.51%	67.48%	68.14%	66.17%	66.76%
Flow fibre volume fraction	55.97%	61.74%	59.57%	63.01%	64.53%	55.55%	57.72%
Number of defects healed	0	0	0	1	0	0	0

A.2.3. Coupons with 90° defect

Coupons / Parameters	90G1.05	90G3.05	90G4.05	90G7.05
Gap – total (µm)	N/A	137.21	N/A	903
Gap pre vs. post cure (µm/ µm)	N/A	10.80%	N/A	71.10%
Overlap total length (µm)	N/A	1366	N/A	1692
Overlap pre vs. post cure (µm/ µm)	N/A	107.57%	N/A	133.21%
Overlap shear flow (µm)	N/A	2374	N/A	1896
Overlap max thickness (µm)	N/A	173	N/A	248
Gap fibre volume fraction	N/A	42.07%	N/A	38.66%
Overlap fibre volume fraction	N/A	69.31%	N/A	67.97%
Flow fibre volume fraction	N/A	64.37%	N/A	59.85%
Number of defects healed	1	2	4	4

Link between Chapters 2 and 3

In Chapter 2, strengths of laminates with half gap/half overlap were determined experimentally. Detailed microscopy analysis was conducted to determine defects' internal structure. Post cure, the defect's regions were delineated as gap, overlap and flow. The plies above and below the defect exhibited waviness, which increased with the number of defects. Waviness is one of the important characteristics that affects the maximum tensile and compressive strengths of the laminates.

Models need to incorporate defect's internal structure to accurately predict the strength of laminates. In Chapter 3, various models are investigated. The first two models (made using cohesive elements and cohesive interaction by previous graduate students) do not incorporate waviness while the last model is used to generate ply waviness. The results are compared with experiments discussed in Chapter 2 to determine their effectiveness.

3. Models to study the effect of gap/overlap defects on the strength of composite structures fabricated using automated fibre placement (AFP) method.

Cadran, V.[1], Del Rossi, D.[1], Thakur, P.[1], Palardy-Sim, M.[2], Lapalme, M.[3] and Lessard, L.[1]

[1] Department of Mechanical Engineering, McGill University, Montreal, Quebec Canada H3A 0C3

[2] National Research Council Canada, Aerospace Manufacturing Technology Centre, 2107 ch. de la Polytechnique Montreal, Quebec, Canada, H3T 1J4

[3] Bell Textron Canada Limited, 12800 rue de l'avenir, Mirabel, Québec, Canada J7J 1R4

Abstract

Automated fibre placement (AFP) is a method used to create large or complex composite parts with the help of a computer-controlled arm capable of constant placement of uncured pre-impregnated carbon fibre tows grouped together to form bands. While it has its advantages in terms of speed and precision, it also leads to defects in the parts that are not seen in other methods. Primary defects observed by the aerospace industry are misaligned tows, often the result of trying to steer the tows. These defects lead to design uncertainty, which must be examined from both an experimental and theoretical modeling perspective. In this second part of this two-part paper, finite element simulation models are used to predict the effects of steered tow defects on the tensile and compressive strengths of composite structures made with AFP.

Various finite element simulation models are considered with and without inclusion of fibre waviness and the results are compared to the results obtained from experiments in the first paper [1].

3.1 Introduction

Composite structures are used extensively in the aerospace industry due to their high strength- to-weight ratio. Two of the main automated technologies that use advanced composite laminates are Automated Tape Laying (ATL) and Automated Fibre Placement (AFP). These use material in the form of unidirectional (referred as UD) pre-impregnated fibres (prepregs) [2,3]. Manufacturing experience has shown that the AFP machines are not perfect. They tend to create a variety of defects, which end up being embedded in the laminate [4]. In Paper 1 [1] of this two-part paper, an experimental investigation was performed to examine the tensile, compressive and fatigue performance of laminates with varying defect configurations (number, size and orientation of defects). The experimental test matrix could not cover all possible configurations of defects and stacking sequences, but many key observations were noted [1]. To support the experimental findings, a Finite-Element (FE) model is used to simulate laminates with embedded defects in static tension and static compression. The main goal to have the ability to predict the behaviour of any configuration in the future. This modeling work follows a novel approach to represent the post cure defect geometry that was experimentally observed in [1].

Several models exist in the literature for predicting the strength of composite structures with defects. Blom et al. [5] developed numerical models to explore mechanical performance of AFP-manufactured composite structures with defects. The study considered tow drop areas where gaps are created due to fibre curvilinear path planning. The model used the maximum stress criterion adapted to consider non-linear shear behavior and progressive energy-based damage of fibres. The authors showed important tensile strength knockdowns up to 20% corresponding to regions with maximum 10% tow drop per area.

Heinecke et al. [6] examined in the structural behavior of AFP composite panels with three types of defects: narrow gaps, wide gaps, and wide overlaps that are present between each tape laid down by the AFP head. They used three approaches: analytical based on the rules of mixtures, virtual testing (finite element modelling with delamination fracture mechanics), and multiscale analysis (finite element modelling with simplifications). The stiffness matrix of prepreg was degraded once the failure criterion was reached which led to progressive damage propagation. The authors showed that depending on the modelling method and the choice of failure criterion, results varied slightly and the fracture initiation changed. Gaps reduced stiffness and strength by 10% to 20% while for the overlap configuration, the observed knockdown was 22% compared to baseline defect-free laminates. However, as the authors pointed out, waviness was not considered and out-of-plane effects could lead to different results.

Fayazbakhsh et al. [7, 8, 9] studied the effects of single gaps and single overlaps with finite element modelling using a new method called the "defect layer method". The FEA study [9] used two different composite designs based on different buckling and in plane stiffness objectives. The defect layer method was used to represent the appearance of gaps or overlaps. The defects were spaced out though the entire part and their locations were decided by an algorithm which could predict the appearance of a gap or an overlap based on the properties of the AFP machine, the properties of the prepreg and the fibre path chosen. The model predicted that gaps reduced buckling capability by an average of 12% and overlaps increased it by an average of 30%. Gaps reduced in plane stiffness by an average of 14% while overlaps increased it by an average of 10%. These numerical results were not thoroughly validated by experiments.

Marrouze and Abdi [10, 11] defined the multi-scale progressive failure analysis (MS-PFA) approach to study the effects of gaps on the mechanical performance of composite structures. In this approach, once the tensile, compressive and shear properties of the element with defects are characterized, the unit cell is integrated into a larger macroscale structure in a Finite-Element model following a specific gap distribution. MS-PFA approach considered damage initiation and damage energy-based evolution of a crack based on strain and strength formulations. Plies were modeled with delamination capabilities using cohesive interactions. The authors concluded that the degradation of material properties was due to fibre waviness. However, increasing the length of the gap did not increase knockdown factors.

In 2015, Xianqian, Hallet and Winsom [12] used their previous model with a Weibull failure criterion [13] and element removal approach of progressive damage mechanism to assess the effects of defects made by the AFP manufacturing process. Single gaps, single overlaps and a mix of both gaps and overlaps were studied both numerically and experimentally. This model used a ply-by-ply analysis on LS-DYNA software in both tension and compression. The laminate modelling algorithm considered ply waviness with hard tooling (using caul plates) and soft tooling (without caul plates) during the cure cycle. Modelling results showed that single gaps and single overlaps caused larger knockdown in compression – an average of 20% – than in tension – an average of 10%. Embedded defects in +45° or -45° oriented plies had more effect than in 90° plies. The strength knockdown caused by gaps was larger than the strength knockdown caused by overlaps.

Nartey et. al. [14] used the pre-processing tool in [12] to perform numerical simulations and studied the effect of wrinkle architecture on deformation and failure mechanisms. Cohesive elements were used using the constitutive laws outlined in [15]. The authors concluded that the wrinkle angle increased with the number of defect plies and decreased with increasing gap width. Tensile strength dropped by a maximum of 21% and compressive strength dropped by at most 37%. The model was verified with experiments and yielded good agreement.

Recently, Ghayour et al. [16] investigated the effect of fibre tow gaps (created using AFP) on the impact response of carbon/epoxy laminates and developed a semi-analytical model to predict the effect of manufacturing induced defects on the impact response of the composite plates. The proposed model's results were in good agreement with experiments for low level of impact energy. The authors also studied the effect of AFP induced gaps on the mechanical response and failure of the Quasi-isotropic Carbon/Epoxy thin beams under out of-plane loading [17] and found that the flexural stiffness of the beam reduces by around 35% due to fiber tow gaps. They concluded that thickness scaling is as important as material scaling to model the out of plane loadings.

Jamora et. al. [18] employed digital image correlation to measure the thermal expansion coefficients of AFP lamina and used them in a FEA model to simulate the cooling phase of the cure cycle and the resulting residual stresses. The predicted residual deformation was analyzed considering out-of-roundness in cylindrical shells and compared to experimental results. The shell FEA results correlated well with the overall deformed shape of the AFP cylinder with overlaps, but the results of the shell FEA model of the AFP cylinder without overlaps did not show such a good match. The effect of roller diameter on the formation of wrinkles during placement of tows

over a flat surface was studied using experiments and simulations by S. Rajan et. al [19]. They found good agreement between the experiments and the model's prediction of wavelength and amplitude of wrinkles for straight and curved paths.

It is clear from the literature that defects have influence on AFP material strength, and that fibre waviness may play a key role. Most of the above models considered above contain defects through the entire width of the laminate. However, these defects do not represent the actual geometry of a misaligned tow, which often has a finite size. The majority of the defects encountered in manufacturing are half gap/half overlap defects [20]. The present paper develops models to predict the tensile and compressive strengths of laminates containing half gap/half overlap defects which do not go though the entire width of the laminate.

3.2 FEA Model I: using cohesive interaction

Industries currently rely on experimental tests to determine knockdown factors of laminates with gap/overlap defects. As not every defect configuration can be tested, it is important to create a finite element model that can simulate tests on these laminates. The model discussed in this section uses cohesive interaction between plies as opposed to cohesive elements. Modeling with cohesive elements is discussed in the next section 3.

3.2.1 Model assembly

When simulating composite parts, the assembly is made to match the real-life parts and then the composite layup is applied to each part. This method works well for most parts, but it does not

capture the out-of-plane effects between plies. Usually, this is not a problem, but in the case of AFP defects the out-of-plane loads need to be captured. Thus, each ply was initially modelled separately and then attached together with cohesive interactions. This allowed more freedom in the model, and more importantly, it allowed for half gap/overlaps to be incorporated into individual plies. However, the model required a long time to complete simulations (sometimes in the order of days when 10 defects were included). In order to reduce the computational time, a simplified version was created and verified with the initial model to ensure that the results were the same. The simplified model would group adjacent plies without defects together into one part (Figure 3.1). This reduced the amount of parts, and more importantly reduced the number of cohesive interactions, which was the main cause of long simulation times.

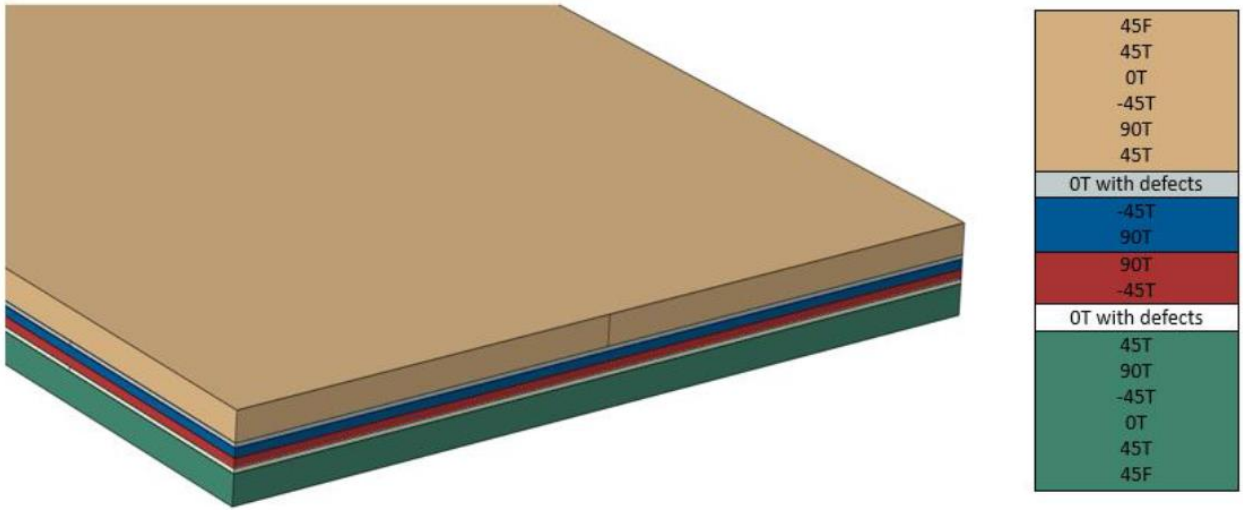

Figure 3.1: Example of grouping plies without defects

In order to model the half gap/overlap defect, some simplifications were made. First, the shape was simplified to the shape of a trapezoid as seen in Figure 3.2.

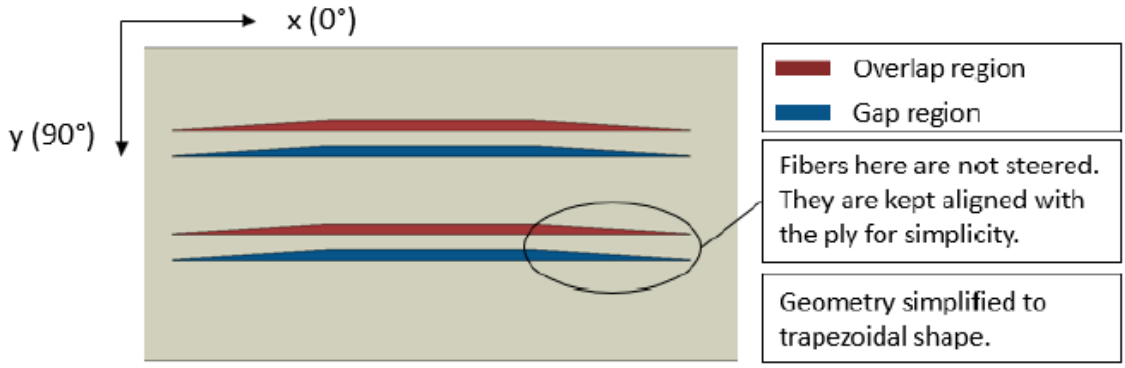

Figure 3.2: Model defect geometry: two half gap/overlaps shown

The gray area shows the prepreg tows, but individual tows are not shown because they are not modeled separately. The blue region has neat resin properties, and the red is a prepreg material with some modifications to reflect the change in the fibre volume fraction. Thickness of both the regions is assumed to remain unchanged. The fibres in the entire ply were all assumed to be along the intended fibre orientation. In reality, there is some fibre steering in transition regions, but it is very minimal and so it is ignored to simplify the model.

It is difficult to test the specific defect regions (gap/overlap) and find out their exact properties. However, the rule of mixtures formulas can be applied to a few of the properties in order to estimate their values. Equations 3.1 to 3.4 specify the rule of mixture formulas used.

$$E_{11} = (1 - V_f) * E_m + E_f * V_f \quad 3.1$$

$$X_t = (1 - V_f) * X_m + X_f * V_f \quad 3.2$$

$$\frac{1}{E_{22}} = \frac{1 - V_f}{E_m} + \frac{V_f}{E_f} \quad 3.3$$

$$\frac{1}{Y_t} = \frac{1 - V_f}{Y_m} + \frac{V_f}{Y_f} \quad 3.4$$

Where:

E_{11} , E_{22} = composite longitudinal and transverse modulus

V_f = fibre volume fraction

E_m = neat matrix modulus

E_f = neat fibre modulus

X_t = composite longitudinal tensile strength

X_f , X_m = tensile strength of the neat fiber and matrix

Y_t = composite transverse tensile strength

Y_f , Y_m = tensile strength of the neat fiber and matrix

Equations 3.1 to 3.4 are used in the different regions after estimating the fibre and matrix volume fractions in these regions.

3.2.2 Failure criteria

Progressive damage was used for the failure of composite plies. There are multiple criteria to evaluate the failure of composite parts, such as the maximum stress criteria and the Tsai-Wu quadratic interaction criteria. While these are all valid methods for evaluating static laminate failure, the Hashin failure criteria was chosen within the FEA software Abaqus. The plane stress Hashin failure criteria evaluates the condition of a laminate by looking at 4 failure modes [21]. These 4 modes are the fibre tension, fibre compression, matrix tension, and matrix compression modes. Equations 3.5 to 3.8 govern these failure modes.

$$\left(\frac{\sigma_x}{X_T}\right)^2 + \left(\frac{\sigma_s}{S}\right)^2 = 1 \qquad \sigma_x > 0 \tag{3.5}$$

$$\sigma_x = -X_c \qquad \sigma_x < 0 \tag{3.6}$$

$$\left(\frac{\sigma_y}{Y_T}\right)^2 + \left(\frac{\sigma_s}{S}\right)^2 = 1 \qquad \sigma_y > 0 \tag{3.7}$$

$$\left(\frac{\sigma_y}{S}\right)^2 + \left[\left(\frac{Y_c}{2S}\right)^2 - 1\right]\frac{\sigma_y}{Y_c} + \left(\frac{\sigma_s}{S}\right)^2 = 1 \qquad \sigma_y < 0 \tag{3.8}$$

Where

- σ_x, σ_y, σ_s = longitudinal, transverse and shear stresses
- X_T, X_C = longitudinal tensile and compressive strengths
- Y_T, Y_C = transverse tensile and compressive strengths
- S = shear strength

3.2.3 Boundary conditions and loading

The boundary conditions were chosen to simulate laminates matching the experimental set up for both compression and tension. One end of the laminate is constrained in x-translation while the other end is prescribed with a constant displacement rate. To avoid rigid body motion, two nodes are constrained in z-translation and one node is constrained in y-translation, as shown in Figure 3.3, on each side of the laminate. All rotations are allowed. The chosen constraints allow for Poisson ratio effects, avoiding artificial stress concentrations due to boundary conditions.

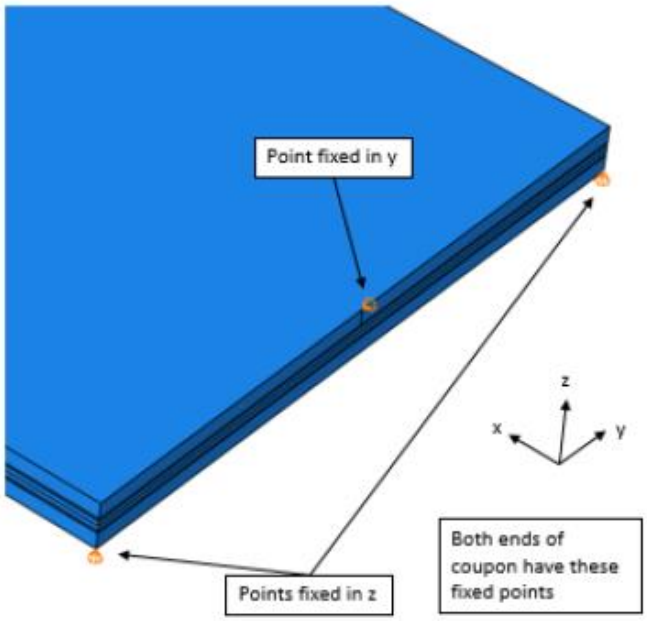

Figure 3.3: Fixed point boundary conditions

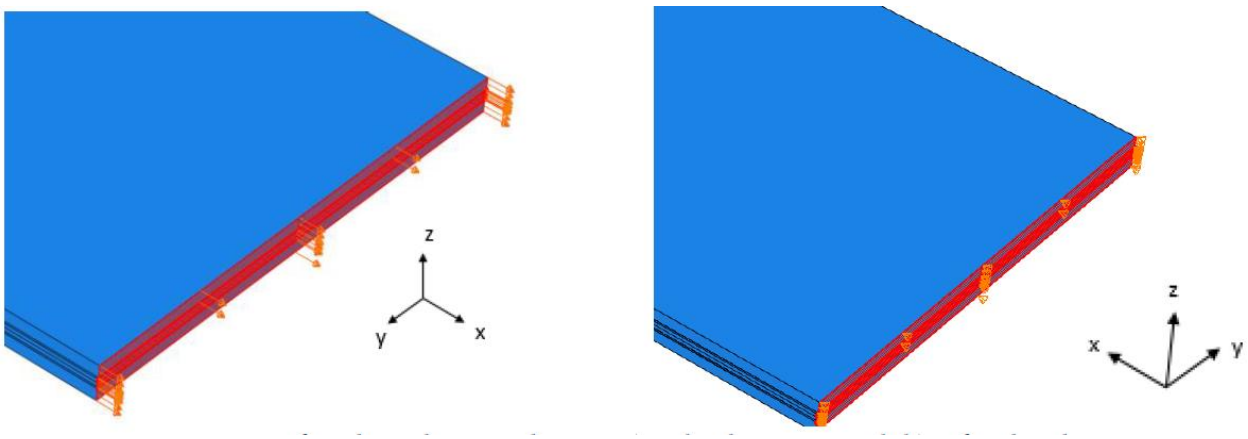

(a) **(b)**

Figure 3.4: Surface boundary conditions. (a) x-displacement end, (b) x-fixed end

3.2.4 Mesh

Due to the presence of defects in the model, the geometry makes it difficult to obtain a uniform mesh throughout the laminate. Also, since the plies with defects are modeled separately from the rest of the laminate, two meshes coexist in the model. The plies with defects have a complex mesh with refined regions. Continuum shell elements SC8R and SC6R with reduced integration, enhanced hourglass control and second order accuracy were used to model the plies.

The model employed mostly hexahedral element geometry. It was observed that the irregular mesh had a negative effect on the results of the simulations. Thus, extra controls were put in place to guide the mesh in the defect area while still giving the software room to generate a suitable mesh. The defect area was partitioned from the rest of the coupon. The ends outside of this partition maintained a uniform rectangular mesh. Inside the defect zone, the sizing of the mesh was reduced to allow for easier node generation around the thin defects. Hexahedral continuum shell elements were used as much as possible but triangular elements could also be used. Use of the hex-

dominated mesh removed the issue of the mesh affecting the results and it also removed the appearance of elements that had excessive distortion. Using only triangular elements was tested also, but it led to too many excessively distorted elements. An example of the final mesh can be seen in Figure 3.5. The figure shows a 90° ply with two half gap/overlap defects. The red areas are overlaps and the blue areas are gaps (as previously explained in Figure 3.2). Even though the tip regions of the defects cause some increased node density, it is not enough to harm the simulations.

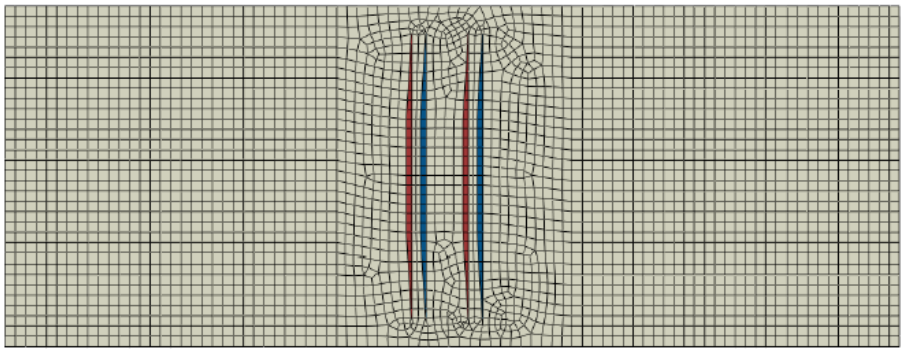

Figure 3.5: Example of mesh for 90°ply containing defects

During manufacturing, the ply waviness (caused by the AFP layup) is reduced because of the use of hard tooling, but it is still significant. Since defect geometry tends to change post cure, which could also have an influence on the model results, another model was created which used the post cure dimensions obtained from microscopy in [1]. It was also believed that cohesive elements would better model the resin in between the plies since it is closer to the geometrically. Hence, the new model incorporates cohesive elements.

3.3 FEA Model II: using cohesive elements

3.3.1 Model assembly

The 3D model follows a ply-by-ply approach with consecutive plies connected using a cohesive layer to allow for debonding and delamination. Since the manufactured laminates had 18 plies [1], the model was composed of 18 plies joined with 17 cohesive layers. The thickness of the cohesive layers was obtained from microscopy [1] and the thickness of the plies was obtained from the manufacturer's datasheet [22]. An interface interaction is used to tie the nodes of two consecutive layers that are in contact.

Similar to model I, material properties of defect regions were obtained from the rule of mixtures and the Hashin failure criteria was used to predict ply failure. Loads and boundary conditions were the same as model I for both tension and compression. However, for compression, the nodes of the top and bottom surfaces of the laminate were constrained in the normal direction, except for a small rectangle corresponding to the fixture D6484 window, to represent the effects of the anti-buckling fixture that was used in testing [1].

3.3.2 Mesh

Model II used a mesh similar to that of model I, with the mesh size in the defect region being four times smaller than the mesh size of defect-free regions. Triangular elements were used to make a clean transition between the regions, because of the difference between the two mesh sizes. Cohesive layers were modeled by COH3D8 and COH3D6. Other settings such as the solver options were left to their default values. The high stiffness gradient between the gap and the overlap regions induces shear stresses. To accurately analyze the through thickness shear stresses

that propagate the effects of defects onto nearby plies, each layer was composed of three elements in the normal direction.

3.3.3 Progression of ply failure for model II

Ply failure is modeled to occur in progressive steps. For example, for the case of 0° oriented defects configurations, the model final failure occurs earlier than for defect-free configurations. Fibre crack propagates from the embedded defects to the edges of the 0° defect ply as shown in Figure 3.6.

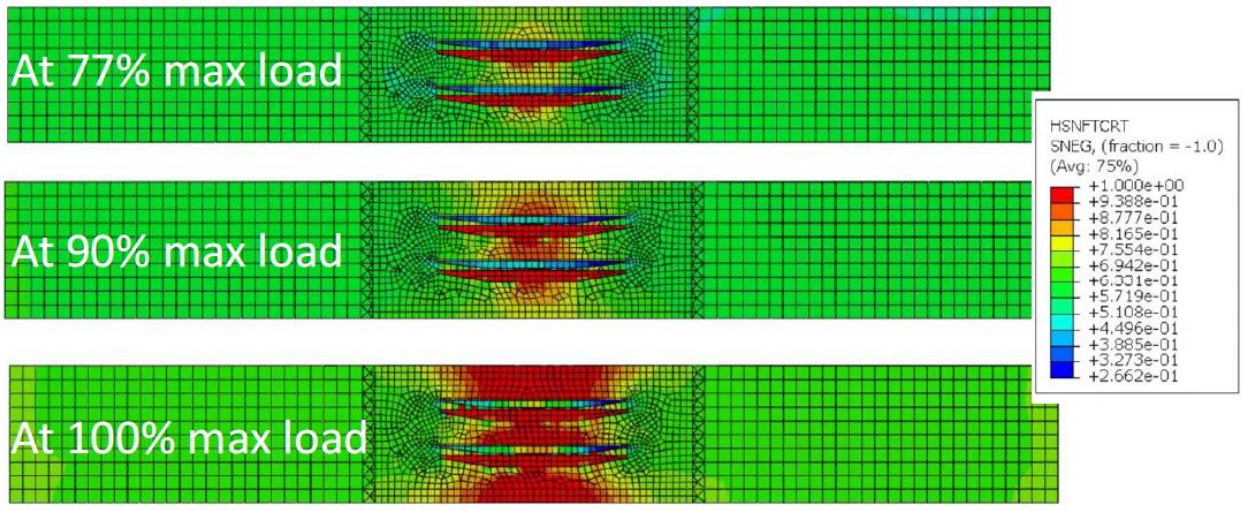

Figure 3.6: Hashin fibre tension: crack propagation in 0° defect ply

Once defects start to fail, delamination around them progresses. As revealed by the DIC results [1], delamination initiates very early in the simulation, starting at the edges before the defect plies fail and the two regions of delamination grow towards each other. In 45° and 90° oriented defect configuration models, all plies fail similar to the defect-free configuration, without any specific

stress concentration region. Transverse shear propagates with some stress through the thickness of the laminate, but it is not enough to change the final mechanical strength of the laminate.

The compression model predicts similar failure initiation and damage propagation as did the model in tension. The major difference is that there is no delamination on the edges in the compression model. DIC analysis in [1] tends to correlate with this finding because no large strains appear on the edges. This can be explained by the use of the anti-buckling fixture which limits the normal debonding and displacement at the edges. However, delamination does occur along the defects, for all orientations.

The overlap fails first because it is a stiff region. The crack propagates from the defect region to the edges, as shown in Figure 3.7. 0° plies fail in fibre compression while 45° and 90° plies fail in matrix compression. Even plies without defects fail in the region of defects, at the middle of the laminate.

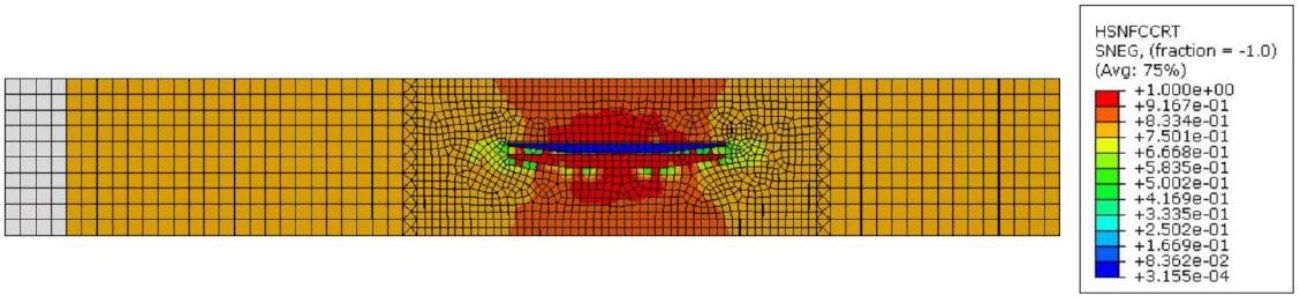

Figure 3.7: Hashin fibre compression in 0° ply with defects, at failure

3.4 Results from Models I and II

3.4.1 Tension test results

The results of tensile strengths vs number of defects predicted by model I (using cohesive interaction) and model II (using cohesive elements) are shown in Figures 3.8 to 3.12. Experimental results from paper [1] are included too for comparison. The values are normalized with respect to the defect free coupons. Each figure corresponds to a specific defect size and orientation indicated by the figure captions.

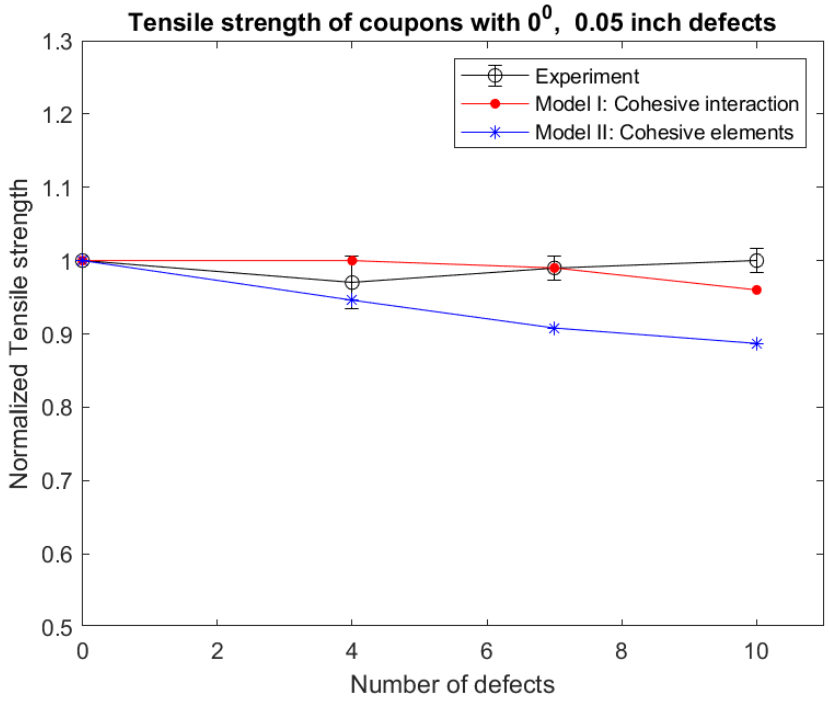

Figure 3.8: Tensile strength of coupons with 0.05" (1.27 mm) wide defects oriented at 0°

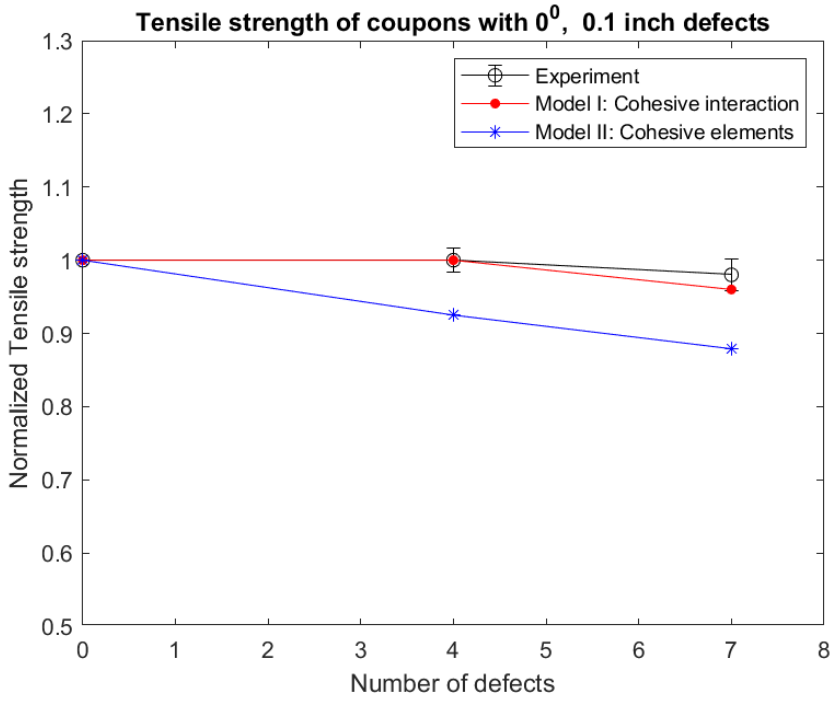

Figure 3.9: Tensile strength of coupons with 0.1" (2.54 mm) wide defects oriented at 0°

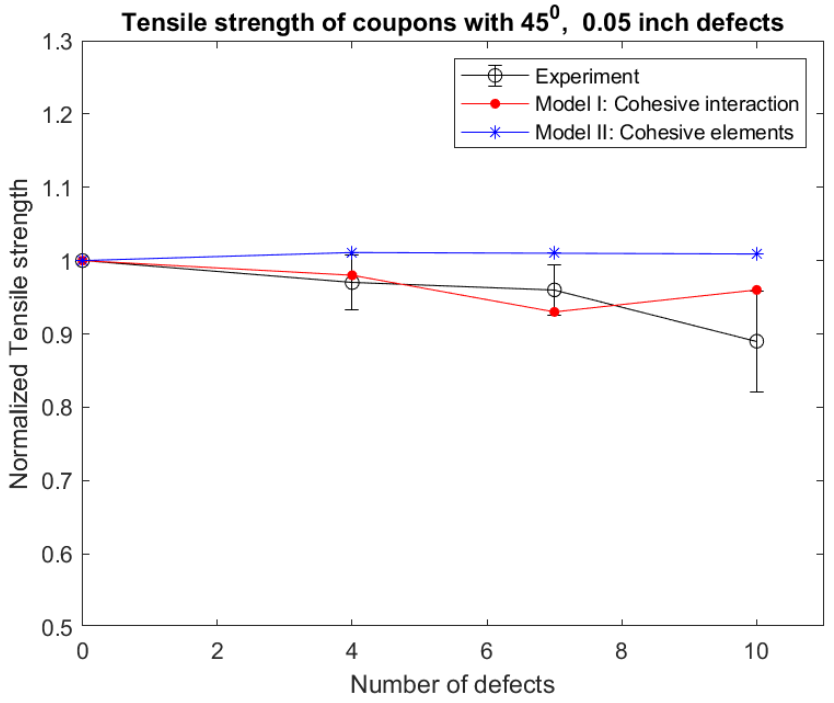

Figure 3.10: Tensile strength of coupons with 0.05" (1.27 mm) wide defects oriented at 45°

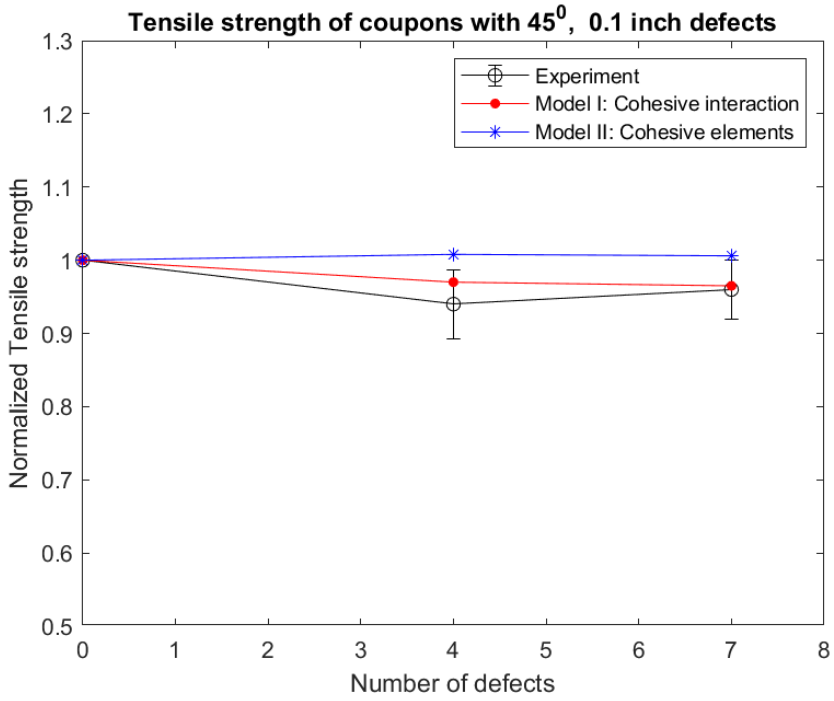

Figure 3.11: Tensile strength of coupons with 0.1" (2.54 mm) wide defects oriented at 45°

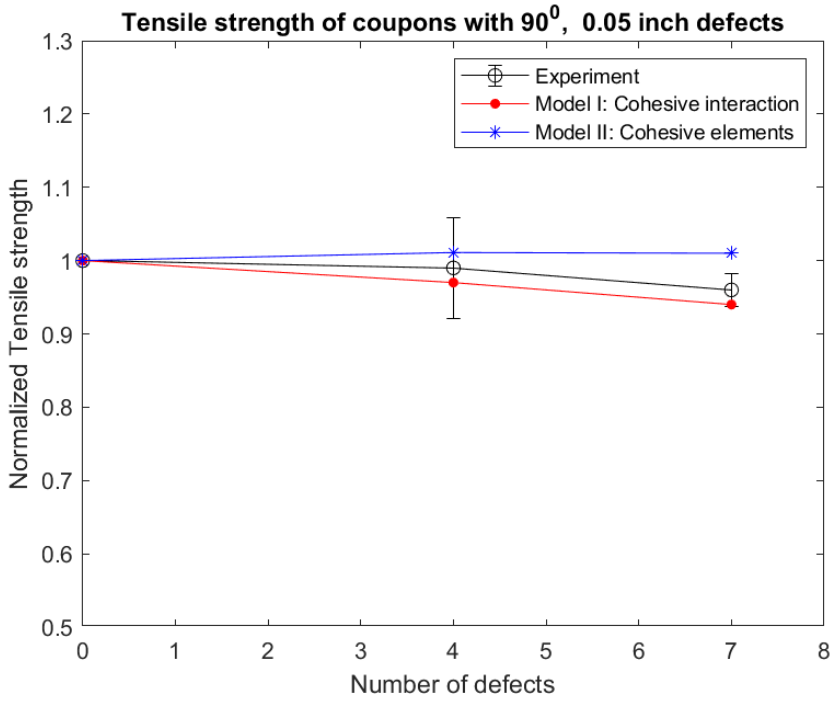

Figure 3.12: Tensile strength of coupons with 0.05" (1.27 mm) wide defects oriented at 90°

As seen from the plots in Figures 3.8 to 3.12, the tensile strengths do not vary significantly with the number of defects. The predictions of both the models are close to the experimental results. While model I appears to be more accurate in predicting the experimental results, the error in both the models is within 10%. However, these models have certain limitations. The trends in 0° defects are not accurately captured by both the models. For example, in 0.05" (1.27 mm), 0° defects, the experimental tensile strength increases with the number of defects while the models predict it to decrease. Model II is not significantly affected by the presence of 45° and 90° defects. These limitations can be explained by the lack of waviness in the models.

3.4.2 Compression test results

The results of tensile strengths vs number of defects predicted by model II (using cohesive elements) are shown in Figures 3.13 to 3.15. Experimental results from paper [1] are included too for comparison. The values are normalized with respect to the defect free coupons. Only 45° and 90° defect coupons were used for the experiments. Each figure corresponds to a specific defect size and orientation indicated by the figure captions. The results from Model I (cohesive interaction) are not shown as it could not be set up to provide accurate results.

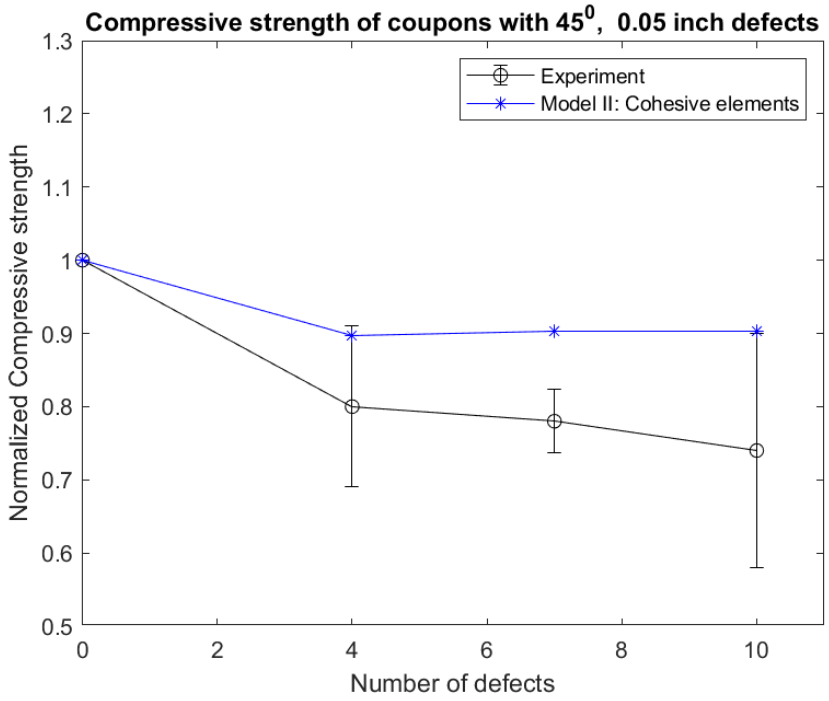

Figure 3.13: Compressive strength of coupons with 0.05" (1.27 mm) wide defects oriented at 45°

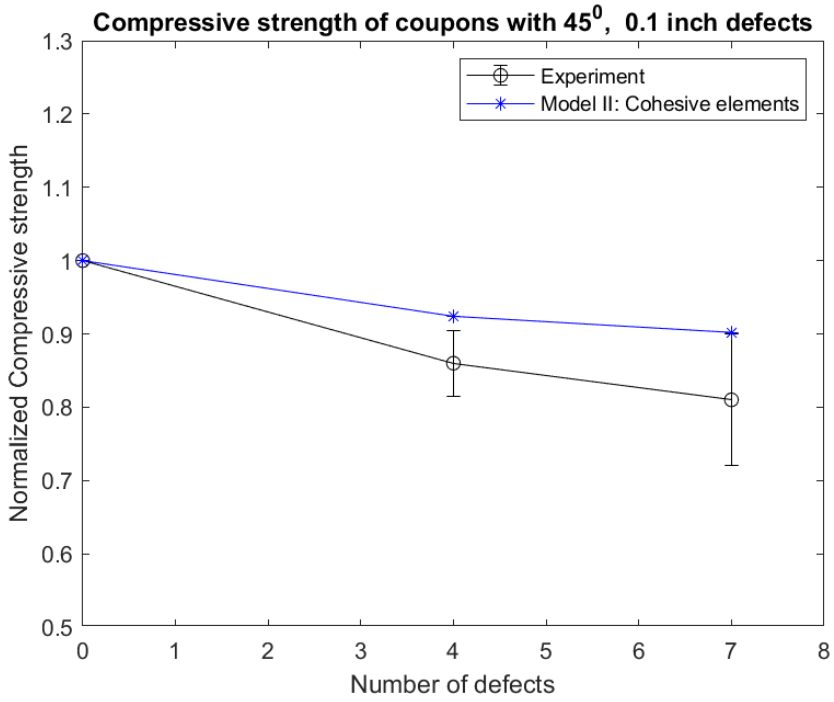

Figure 3.14: Compressive strength of coupons with 0.1" (2.54 mm) wide defects oriented at 45°

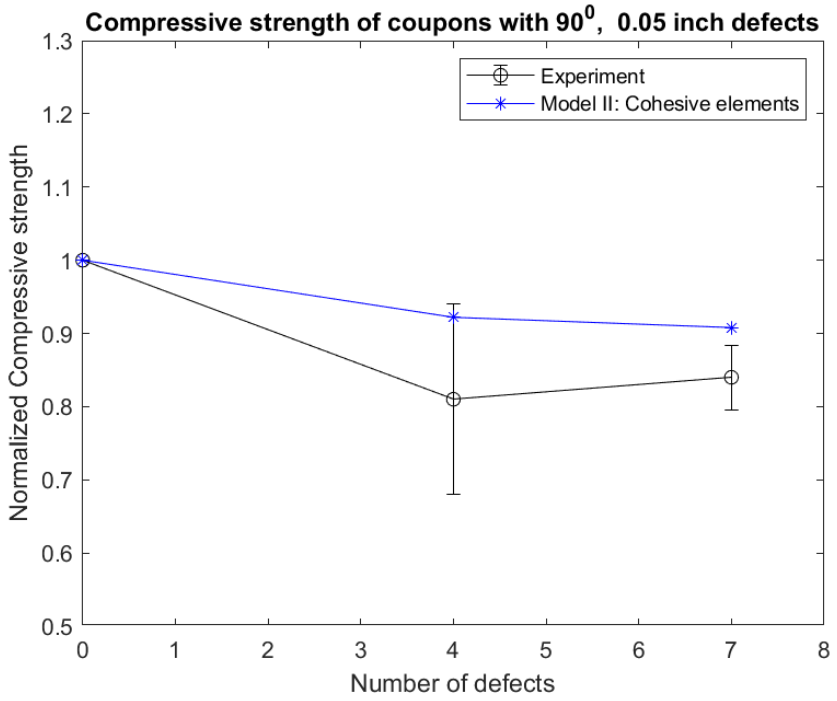

Figure 3.15: Compressive strength of coupons with 0.05" (1.27 mm) wide defects oriented at 90°

As seen from Figures 3.13 to 3.15, the compressive strength reduces significantly (by about 25%) in comparison to the tensile strength due to presence of defects. Model II closely follows the trend of strength reduction in compression. However, it underestimates the magnitude of the reduction. The difference between the experimental results and the model is probably due to waviness, which creates more asymmetry in the laminate structure than the modeled high stiffness (overlaps) and low stiffness (gaps) regions.

The effect of defects can be accurately captured by incorporating ply waviness into the FEA models. Model III in the next section discusses a method to generate laminates with defects and wavy plies.

3.5 FEA Model III: generating ply waviness

3.5.1 Model assembly and meshing

During curing, the plies undergo shear flow and, as shown in [1], with overlaps moving towards the gaps, creating intermediate flow regions. The plies above and below the defects exhibit waviness. The exact wavy geometry of laminates with defects can be obtained by modeling the plies as plastic in Abaqus explicit and seeing how the plies move under out-of-plane pressure loading The initial state of the half gap/half overlap defect was obtained by incorporating the half gap in the defect ply. The half overlap was placed on top of the defect ply and was offset from the half gap by an amount equal to the magnitude of tow misalignment. as shown in Figure 3.16.

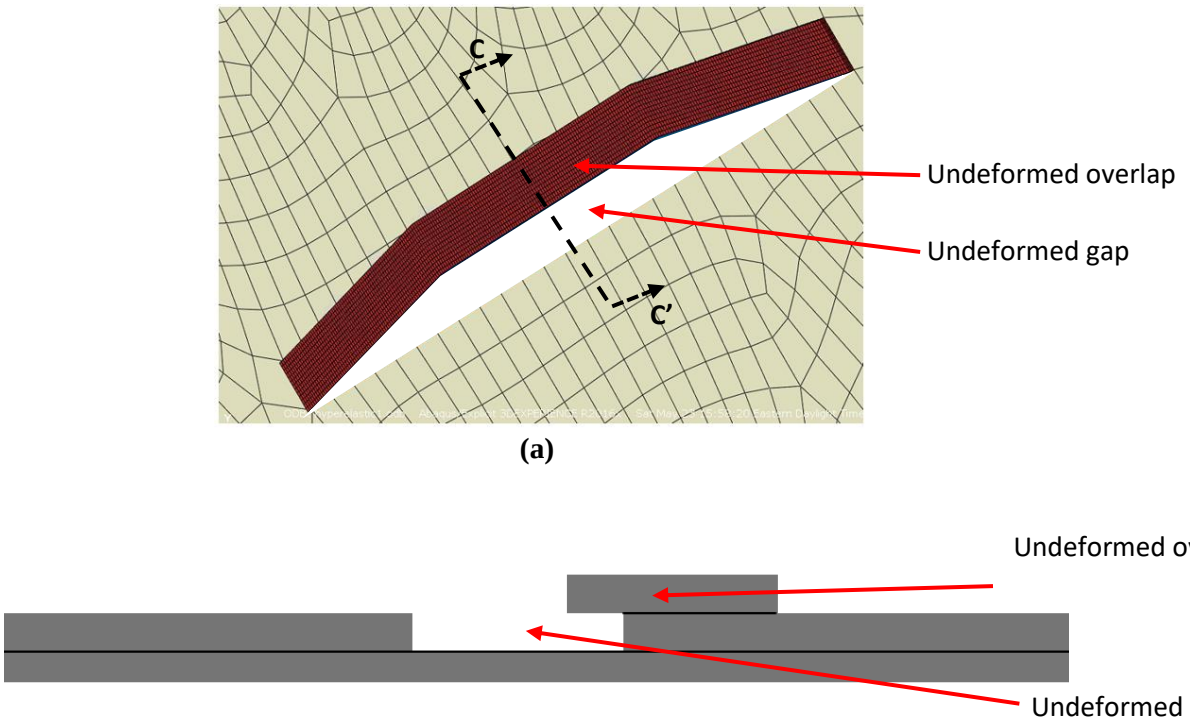

Figure 3.16: (a) Top view and (b) cross section view (along the line CC') of the defect embedded in the ply

All the plies are stacked on top of each other. Figure 3.17 shows the meshed cross section of one of the laminates before simulation. The cross section is taken perpendicular to the defect, similar to Figures 3.16 (a) and (b).

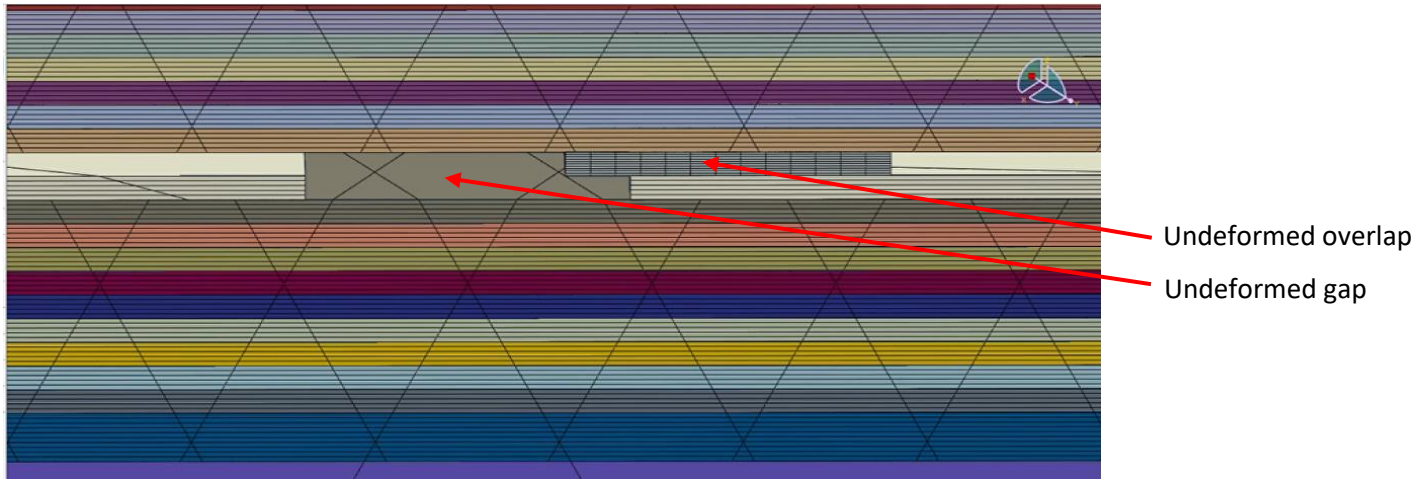

Figure 3.17: Cross section of the laminate before simulation

After stacking the plies, all plies, including overlaps, are assigned a simple plastic property using yield stress and strain. The value of yield stress and strain was chosen to match all the microscopy images as closely as possible. Hex mesh was used with 3D stress elements and reduced integration. The mesh in the overlap region was refined to accurately model the shear flow.

3.5.2 Boundary conditions and results

The stack of plastic plies (laminate) was placed between two large rigid plates (caul plates). Pressure was applied on the top plate while the bottom plate was held stationary, as shown in Figure 3.18.

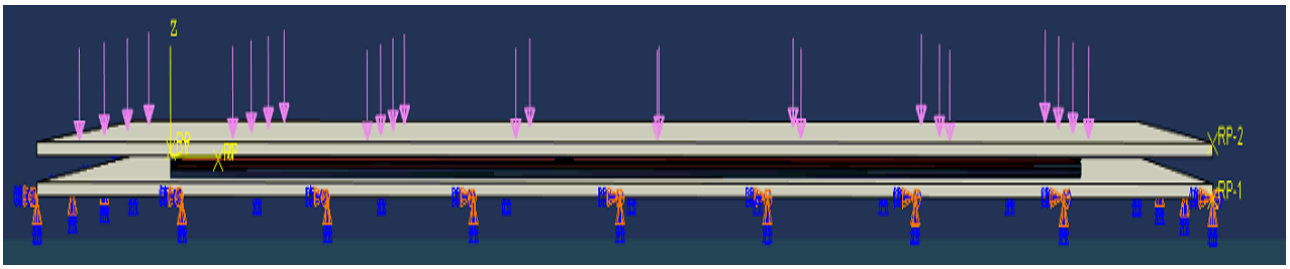

Figure 3.18: Boundary conditions to simulate formation of defects. Image is enlarged to show the laminate in between the rigid plates.

Hard contact interaction without friction was used between ply surfaces. The simulation to generate shear flow was carried out on five different laminates and all of them resulted in geometries similar to the microscopy images, as seen in the examples of cross sections of the laminates in Figures 3.19 and 3.20. Microscopy images are also included for comparison. The cross section was made perpendicular to the defects as done in Figure 3.16.

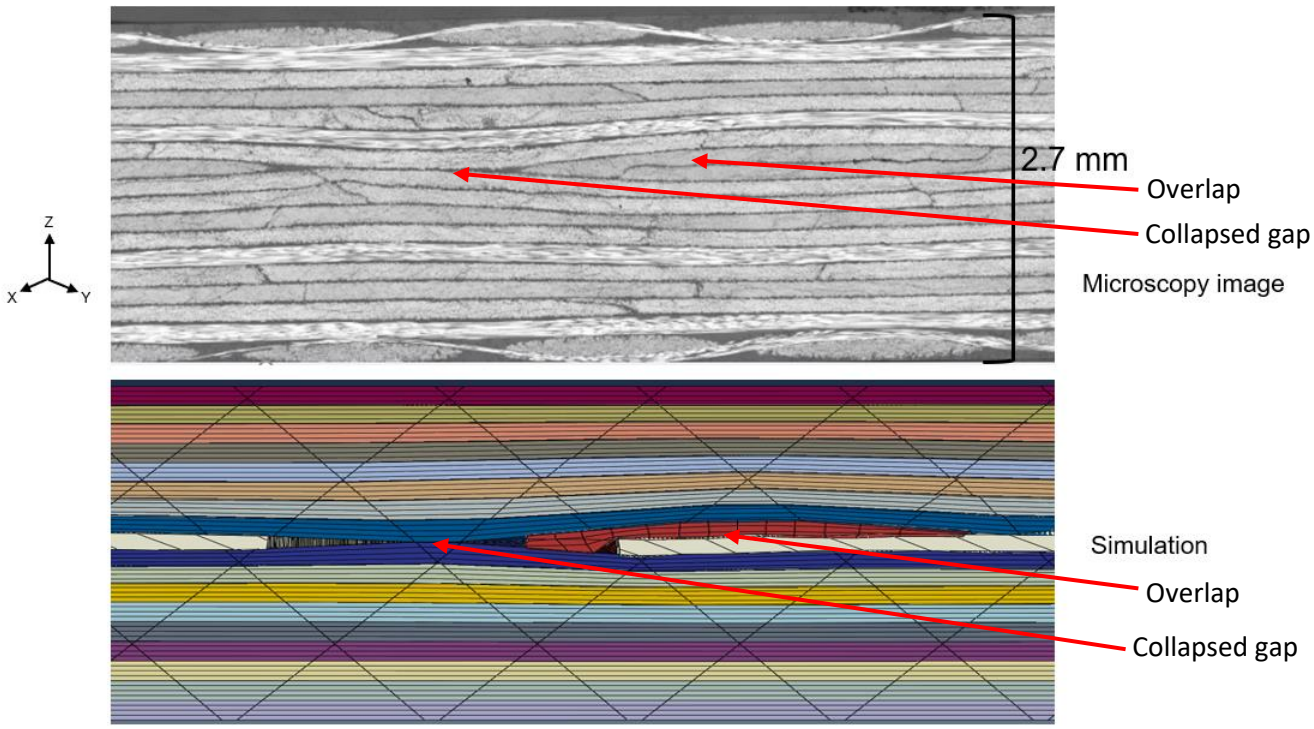

Figure 3.19: Simulation result of laminate cross section containing one 45° defect

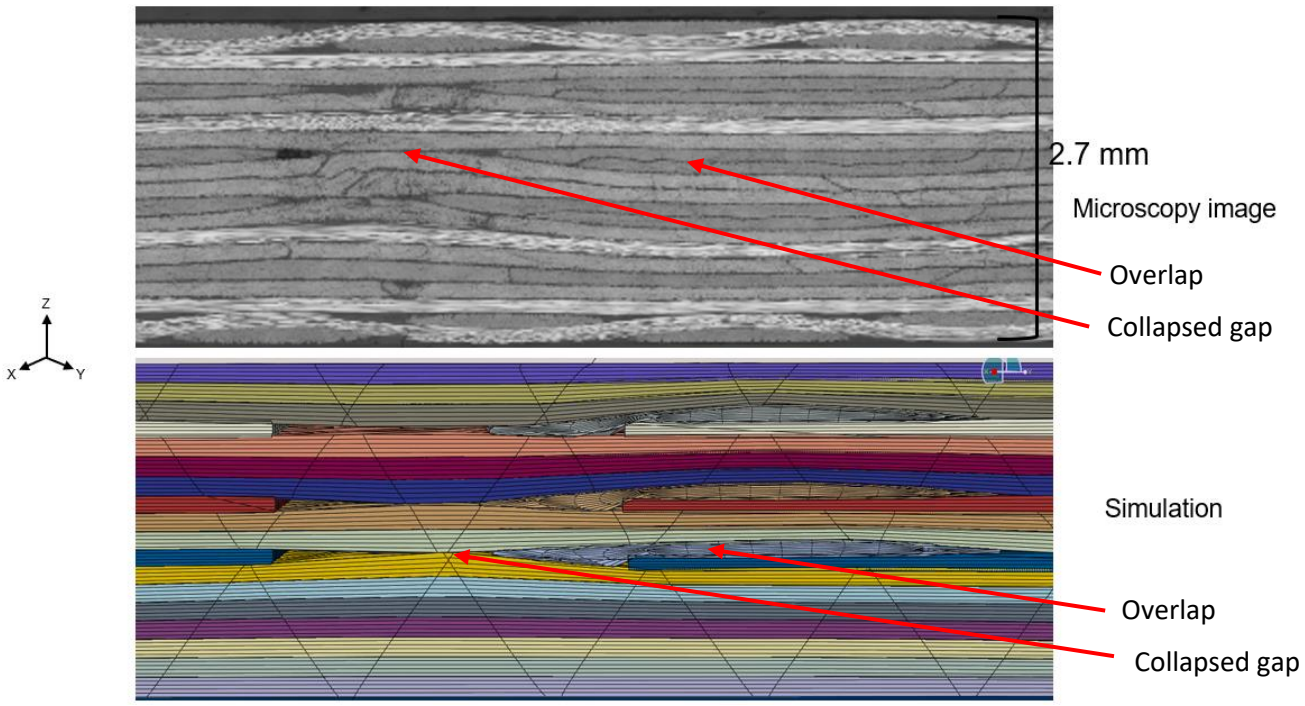

Figure 3.20: Simulation result of laminate cross section containing three 45° defects

0° and 90° defect orientations were also simulated, giving similar results. Thus, the model generates wavy plies which are close to those seen in the microscopy image. There are some differences, however, especially at the top of the overlap. Plies above the overlap in microscopy images are less wavy than the waviness demonstrated by the simulation. This could be due to the simplification of ignoring viscosity changes during curing. Plastic properties of the plies were unchanged throughout the simulation.

3.5.3 Incorporating composite material properties and future work

The deformed geometry of the laminate was exported into a new Abaqus CAE model and each ply was assigned composite material properties separately with the ply orientations specified in [1]. The deformed stack of plies was assembled in the assembly module and converted into a part using a node tolerance such that the plies were well connected but not distorted. Solid mesh elements were converted into continuum shell elements to incorporate Hashin failure criteria. Loads and BCs similar to models I and II were applied. But the tensile and compressive results differed by a large amount compared to the experiments. Close inspection of the laminate revealed that the plies were not well connected. Changing node tolerance while merging the plies did not solve this problem. Low node tolerances resulted in highly disconnected plies while high tolerances distorted the laminate.

An efficient method to implement tie constraints between adjacent plies can improve laminate connectivity and will be explored in the future. Once the wavy plies are well connected, the simulation is expected to provide accurate predictions of the tensile and compressive strengths of the laminates with respect to the experiments.

3.6 Conclusion

Industries are relying on experimental methods to determine the effect of half gap/half overlap defects. However, these methods are inefficient in terms of time and cost and it cannot be used to determine the effect of all possible defect configurations. This paper explored various FEA simulations which can be used to determine a defect laminate's tensile and compressive strengths. Model I and II modeled plies as planar without waviness and changed the material properties of plies in defect regions. Model I used cohesive interaction while model II used cohesive elements to connect the plies. Both of these models indicated that waviness was an important factor in predicting mechanical performance. In order to incorporate waviness into the models, a method of plastic deformation of plies was explored in model III. The deformed geometry of ply stacks was similar to the microscopy image. However, the model gave inaccurate results as the plies were not well connected, despite an attempt to merge adjacent nodes. An efficient method is required to tie/merge the nodes which would improve laminate connectivity and hence create a model which closely emulates the laminates used in experiments.

References

1. Del Rossi, D., Cadran, V., Thakur, P., Palardy-Sim, M., Lapalme, M. and Lessard, L. *Experimental investigation of the effect of half gap/half overlap defects on the strength of composite structures fabricated using automated fiber placement (AFP) method.* Composites Part B: Engineering, 2020 (in press).
2. Lukaszewicz, D.H.J.A., C. Ward, and K.D. Potter. *The engineering aspects of automated prepreg layup: History, present and future*. Composites Part B: Engineering, 2012. 43(3): p. 997-1009.
3. Chen, J., et al. *Manufacturing of composite helicopter tailboom using afp process. in 70th American Helicopter Society International Annual Forum,* May 20 - 22, 2014. Montreal, QC, Canada: American Helicopter Society.
4. Abdi, F., et al. *Certification modeling of composites fuselage, considering effect of defects from fiber placement manufacturing processes. in 55th AIAA Aerospace Sciences Meeting, January 9 - 13, 2017*. Grapevine, TX, United states: American Institute of Aeronautics and Astronautics Inc.
5. Blom, A.W., et al. *A theoretical model to study the influence of tow-drop areas on the stiffness and strength of variable-stiffness laminates*. Journal of Composite Materials, 2009. 43(5): p. 403-425.
6. Heinecke, F., W. Van Den Brink, and T. Wille. *Assessing the structural response of automated fibre placement composite structures with gaps and overlaps by means of numerical approaches.* in *20th International Conference on Composite Materials, ICCM.* July 19 - 24, 2015. Copenhagen, Denmark: International Committee on Composite Materials.
7. Fayazbakhsh, K., et al. *The effect of gaps and overlaps on the in-plane stiffness and buckling load of variable stiffness laminates made by automated fiber placement.* in *15th European Conference on Composite Materials: Composites at Venice, ECCM.* June 24 - 28, 2012. Venice, Italy: European Conference on Composite Materials, ECCM.

8. Fayazbakhsh, K., et al. *A study of the influence of gaps and overlaps on the strength of composite panels made by automated fiber placement.* in *26th Annual Technical Conference of the American Society for Composites 2011 and the 2nd Joint USCanada Conference on Composites.* September 26 - 28, 2011. Montreal, QC, Canada: DEStech Publications Inc.
9. Fayazbakhsh, K., et al. *Defect layer method to capture effect of gaps and overlaps in variable stiffness laminates made by Automated Fiber Placement. Composite Structures*, 2013. 97: p. 245-251.
10. Abdi, F., et al. *Certification modelling of composites fuselage, considering effect of defects from fiber placement manufacturing processes.* in *55th AIAA Aerospace Sciences Meeting*. January 9 - 13, 2017. Grapevine, TX, United states: American Institute of Aeronautics and Astronautics Inc.
11. Marrouze, J.P., J. Housner, and F. Abdi. *The 19th international conference on composite materials effect of manufacturing defects and their uncertainties on strength and stability of stiffened panels*. in *19th International Conference on Composite Materials, ICCM 2013*. July 28 - August 2, 2013. Montreal, QC, Canada: International Committee on Composite Materials.
12. Li, X., S.R. Hallett, and M.R. Wisnom. *Modelling the effect of gaps and overlaps in automated fibre placement (AFP)-manufactured laminates.* Science and Engineering of Composite Materials, 2015. 22(2): p. 115-129.
13. Li, X., S.R. Hallett, and M.R. Wisnom. *A finite element based statistical model for progressive tensile fibre failure in composite laminates. Composites Part B: Engineering*, 2013. 45(1): p. 433-439.
14. Nartey, M., Zhang, T., Gong, B., Wang, J., Peng, S. and Wang, H. *Understanding the impact of fibre wrinkle architectures on composite laminates through tailored gaps and overlaps.* Composites Part B, 2020. 196: p. 1-9.
15. Mukhopadhyay S, Jones MI, Hallett SR. *Compressive failure of laminates containing an embedded wrinkle; experimental and numerical study.* Composites Part A, 2015. 73:132–42.

16. Ghayour, M., Hojjati, M., Ganesan, R. *Effect of tow gaps on impact strength of thin composite laminates made by Automated Fiber Placement: Experimental and semi-analytical approaches*. Composite structures, 2020. 248: p. 1-10.
17. Ghayour, M., Ganesan, M., Hojjati R. *Flexural response of composite beams made by Automated Fiber Placement process: Effect of fiber tow gaps*. Composite Part B, 2020. 201: p. 1-15.
18. Jamora, V.C., Wu, K.C. and Kravchenko, O.G. *Residual deformation analysis in composite shell structures manufactured using automated fiber placement.* Composite Structures, 2020. 248: p. 1-16.
19. Rajan, S. et. al. *Simulations and experiments for automated fiber placement of prepreg slit tape: Wrinkle formation and fundamental observations.* Composite Part B, 2020. 201: p. 1-18.
20. *SA2GE Project*, in *Composite Fuselage Structures*. Bell Helicopter Textron Canada Limited, 2015.
21. Hashin, Z. *Failure criteria for unidirectional fiber composites.* Journal of applied mechanics, 1980. 47(2): p. 329-334.
22. Toray. *Resin system 3900-2*. 2019.

4. Analytical model to predict laminate's strength

4.1 Features of the model

The simulation model with waviness provided a good representation of the geometry of the defect. Waviness from the model was used to create another model to predict the strength of laminates with defects. Classical laminate theory was used along with the stiffness matrix of the wavy plies and plies with defects.

The defect was simplified to be rectangular, as shown in Figure 4.1 (a). Figure 4.1 (b) shows a cross section of the defect obtained from the FEA simulation.

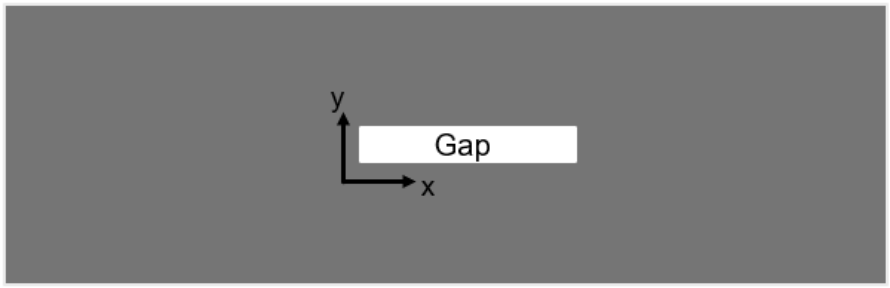

(a)

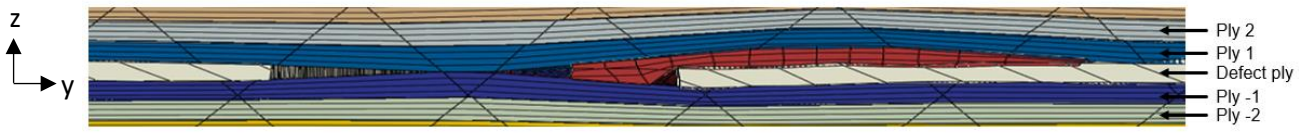

(b)

Figure 4.1: (a) Top view of the gap (b) Cross section perpendicular to the defect in the y-z plane.

Plies above and below the defect (plies 1, and -1 in Figure 4.1) were modeled as sinusoidal in both x and y directions. Stiffness of the plies with defects was calculated using the rule of mixtures with the weights as ratios of lengths of gap, overlap and flow regions.

The stiffness matrix was calculated as follows (ply1 and ply-1 are shown in Figure 4.1 (b)):

$$Ply\ 1 = Ply\ -1 = f(x) \tag{4.1}$$

$$f(x) = A * \sin\left(\frac{\Pi * x}{Gap\ Length\_x}\right) \qquad A: Half\ plythickness \quad x: Distance\ into\ gap\ along\ x.$$

$$Ply\ 1 = Ply\ -1 = f(y) \tag{4.2}$$

$$f(y) = A * \sin\left(\frac{\Pi * y}{Gap\ Length\_y}\right) \qquad A: Half\ plythickness \quad y: Distance\ into\ gap\ along\ y.$$

$$Q_{ply1} = Q_{ply-1} = Average\ stiffness\ of\ the\ wavy\ ply\ modeled\ by\ f(x)\ and\ f(y)$$

$$Q_{ply2} = Q_{ply-2} = \frac{Q_{ply1} + Q_{pristine}}{2} \tag{4.3}$$

$$Q_{defect} = Q_{gap} * Gap\_fraction + Q_{flow} * Flow\_fraction + Q_{overlap} * Overlap\_frac \tag{4.4}$$

With these modified stiffness matrices, classical laminate theory was used with the maximum stress failure criteria and the model ran till all the plies failed. The next section discusses results obtained from the model and compares them with experimental data.

4.2 Results from the analytical model

Tensile strengths predicted by the model for different configurations is shown in Figure 4.2. Figure 4.3 shows the same for compressive strengths. Results from experiments conducted by previous graduate students are also included for comparison. The values of strengths have been normalized with respect to the strengths of defect free laminate. As seen from the Figure 4.2, the model agrees well with experiments in predicting the tensile strength. It also captures the anomaly that some samples with 0° defects exhibit slightly higher tensile strength than defect free laminates.

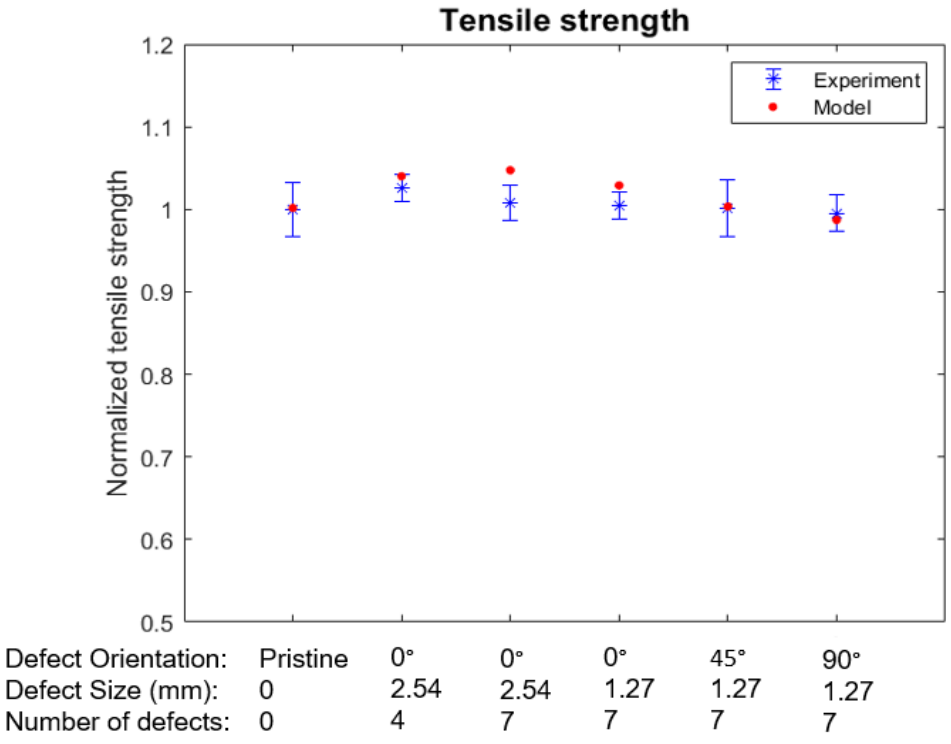

Figure 4.2: Tensile tests: Model vs experiments

From Figure 4.3, it can be seen that the model shows reduction in compressive strengths of the laminates with defects. However, the reduction is not as significant as those indicated by the

experimental data. A major reason for this difference us the lack of delamination in the model. Delamination is more dominant in compression than in tension and can significantly reduce compressive strengths.

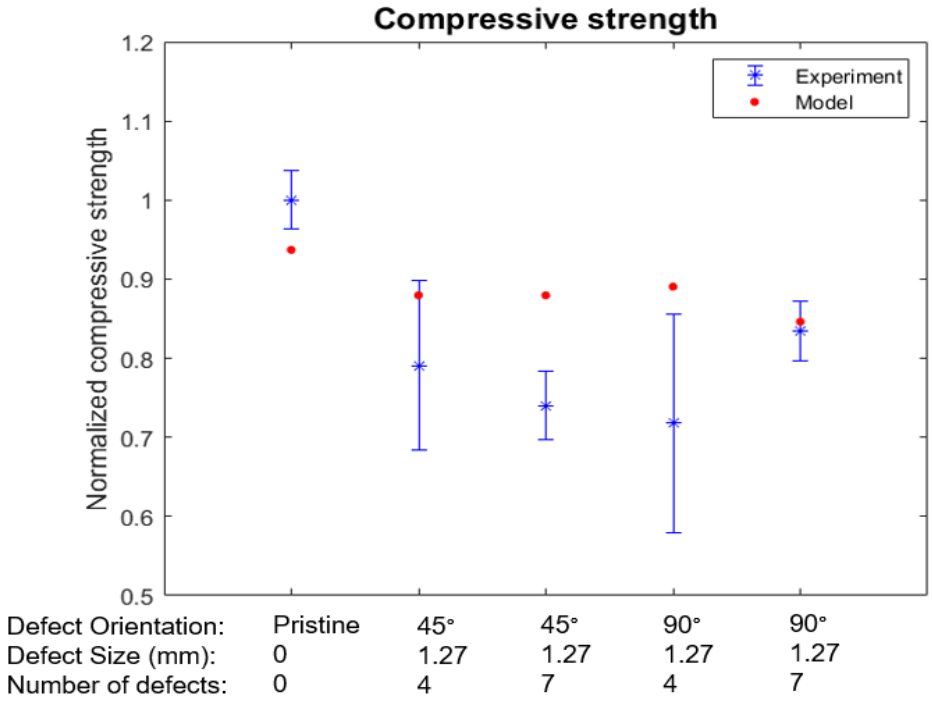

Figure 4.3: Compressive tests: Model vs experiments

As the model gave good results with tensile tests, we can obtain additional data points (tensile strengths of laminates) by varying the defect parameters (i.e. size, number and orientation of defects). The next section discusses these and determines the defect parameter that has the most significant impact on strength.

4.2.1 Effect of defect parameters on the tensile strength

The analytical model gave good results with the tensile tests. We can vary the different defect parameters: size, number and defect orientation, to obtain additional values of tensile strengths. The result has been summarized in table 4.1.

Table 4.1: Effect of defect parameters on the tensile strength

Number of defects	Defect size (inches)	Defect orientation (degrees)	Normalized tensile strength from the Model
0	0	0	1.00
1	0.05	0	0.97
1	0.05	45	0.95
1	0.05	90	0.97
1	0.1	0	0.98
1	0.1	45	0.98
1	0.1	90	0.98
2	0.05	0	0.98
2	0.05	45	0.91
2	0.05	90	0.94
2	0.1	0	1.00
2	0.1	45	0.96
2	0.1	90	0.96
3	0.05	0	1.00
3	0.05	45	0.96
3	0.05	90	0.92
3	0.1	0	1.02
3	0.1	45	0.94
3	0.1	90	0.94
4	0.05	0	1.02
4	0.05	45	1.01
4	0.05	90	0.99
4	0.1	0	1.04
4	0.1	45	0.99
4	0.1	90	0.97

Figures 4.4, 4.5 and 4.6 show the graphs of tensile test data predicted by the model for 0°, 45° and 90° defect orientations. Experimental data available for specific data points are also included for comparison.

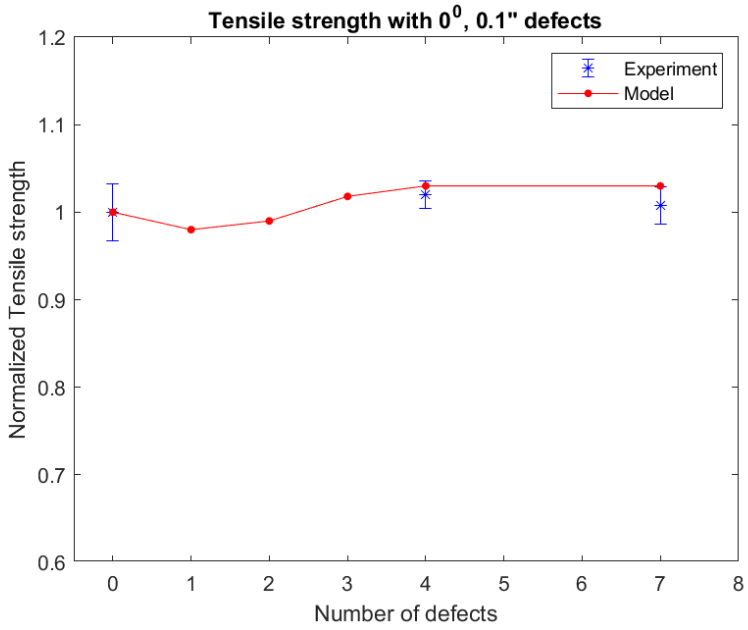

(a)

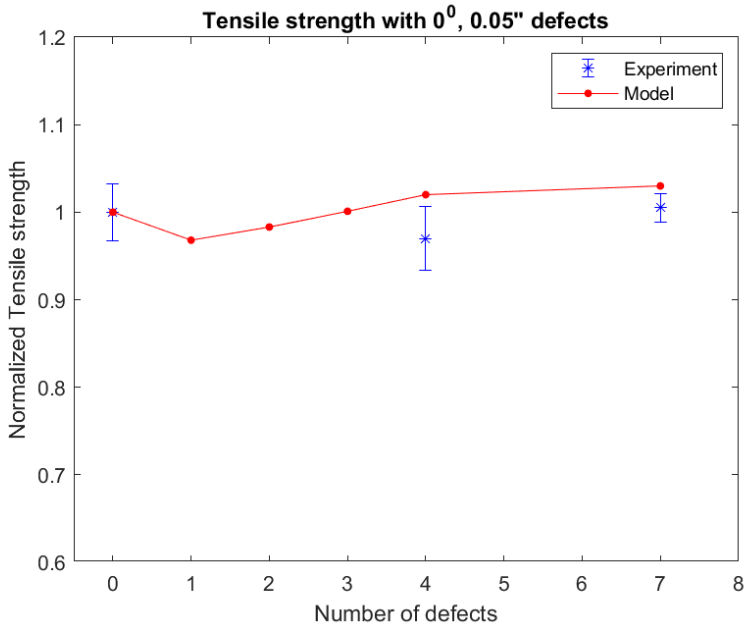

(b)

Figure 4.4: Tensile strength predicted by the model vs number of 0° defects with (a) Defect size of 0.1 inch (2.54 mm) and (b) Defect size of 0.05 inch (1.27 mm)

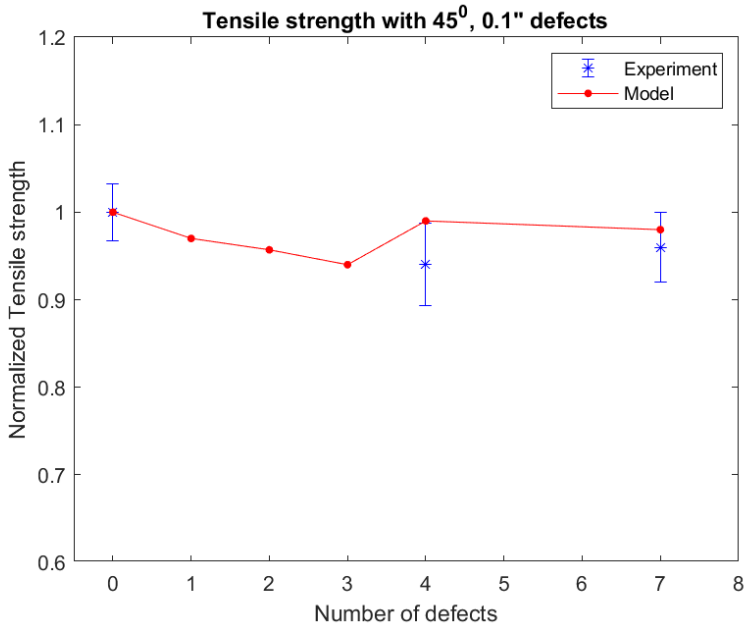

(a)

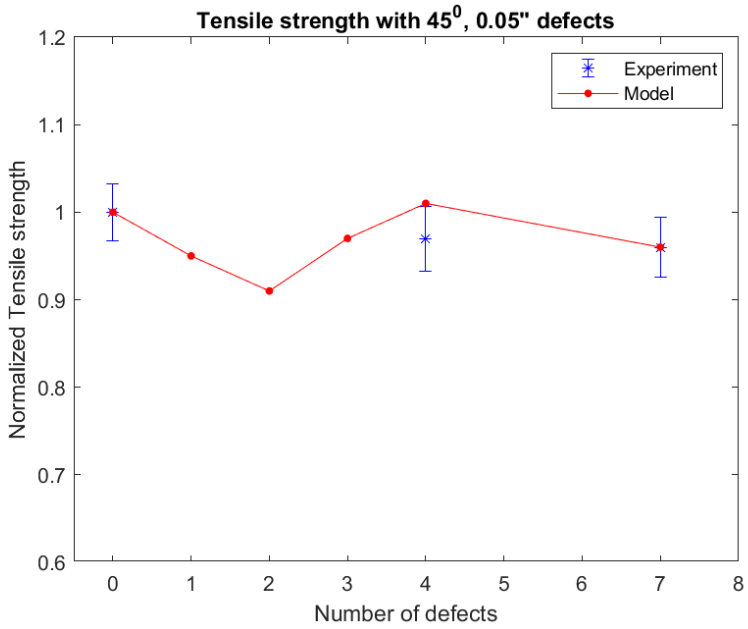

(b)

Figure 4.5: Tensile strength predicted by the model vs number of 45° defects with (a) Defect size of 0.1 inch (2.54 mm) and (b) Defect size of 0.05 inch (1.27 mm)

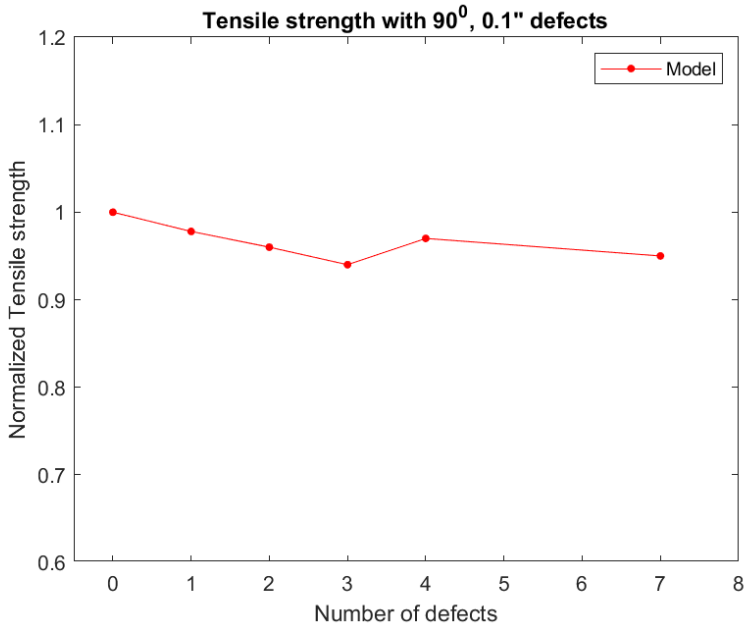

(a)

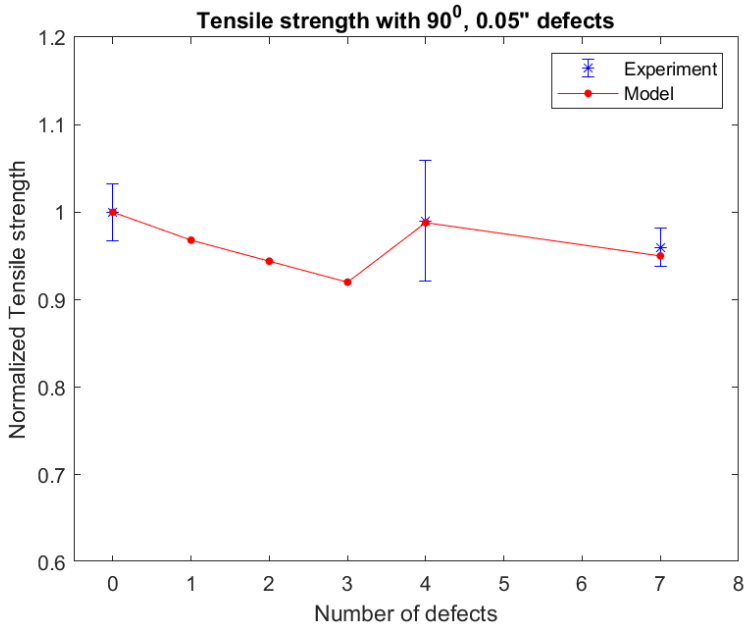

(b)

Figure 4.6: Tensile strength predicted by the model vs number of 90° defects with (a) Defect size of 0.1 inch (2.54 mm) and (b) Defect size of 0.05 inch (1.27 mm)

Having obtained additional data points, we can use multiple regression and fit the data in the following curve, with an associated error of 8 %:

$$T = 0.02N^2 + 0.009N - 0.0046W^2 + 0.007W + 0.013\alpha^2 - 0.019\alpha + 1 \quad (4.5)$$

We can also obtain a linear curve:

$$T = 0.0099N + 0.002W - 0.019\alpha + 1 \quad (4.6)$$

where T is the normalized tensile strength, N is the number of defects, W is the width of defect and α is the orientation of defect. All values are normalized using their z-scores. By comparing coefficients of the equations, it can be concluded that the orientation of defect has the most significant impact on tensile strength, followed closely by the number of defects and the width of defects. This trend is also observed by comparing Figures 4.4 to 4.6.

5. Conclusion

Defects in aircraft structures significantly reduce structure's strengths and it is important to understand their impact on the mechanical performance. To accurately model the effect of defects, microscopy analysis was done on AFP manufactured samples containing half gap/half overlap defects. It was observed that, due to curing, lengths of gaps decreased, lengths of overlaps increased and an intermediate flow region was created due to the shear flow of fibres and resin from overlaps towards the gaps. Based on microscopy conduced on 17 samples, it was concluded that gaps reduced by 64 % on average and overlaps increased by 23 %. Average fiber volume fractions in the gap, flow and overlap regions were 39 %, 59 % and 67 % respectively.

Next, a FEA model was created to replicate the deformation of misaligned tow and to get the defect geometry as seen from microscopy. The model captured the defect geometry and location of failure in tensile tests reasonably well. However, there were issues with element connectivity in the model, as a result of which it underestimated the tensile strength.

Using the defect geometry, an analytical model was created by using the classical laminate theory and taking into account the ply waviness and dimensions of the defects. The model agreed well with the experimental data for tensile tests. Additional data points were generated using this model and, after performing multiple regression, it was concluded that the defect's orientation plays an important role in reducing the strength, followed by the number and size of defects.

6. Future work

In future, the issue of ply connectivity in the FEA model needs to be resolved. An efficient method to implement tie constraints between adjacent plies can improve laminate connectivity. Once the wavy plies are well connected, the simulation is expected to provide accurate predictions of the tensile and compressive strengths of the laminates. Delamination is the dominant mode of failure in compression and it needs to be added to both the analytical and FEA model to accurately predict compressive strengths. To validate the proposed models, additional experimental data needs to be collected with varied defect orientations and sizes. The effect of stacking sequence of the plies and the collective effect of combinations of defects need to be analyzed. For example, a laminate with three defects will have different strengths if the defects are stacked one above the other, rather than being spread out.